Journal of Molecular Liquids 294 (2019) 111626

Contents lists available at ScienceDirect

Journal of Molecular Liquids

journal homepage: www.elsevier.com/locate/molliq

ESIPT-rhodol derivatives with enhanced Stokes shift: Synthesis, photophysical properties, viscosity sensitivity and DFT studies

Sagar B. Yadav, Shantatram Kothavale, Nagaiyan Sekar *

Dyestuff Technology Department, Institute of Chemical Technology, N. P. Marg, Matunga, Mumbai 400019, Maharashtra, India

ARTICLE INFO

Article history:
Received 23 May 2019
Received in revised form 21 July 2019
Accepted 24 August 2019
Available online 29 August 2019

Keywords:
ESIPT-rhodols
Positive solvatochromism
TICT
Viscosity sensitivity
Density Functional Theory (DFT)

ABSTRACT

Three rhodol derivatives, namely spirolactamized phenanthrene-imidazole, diphenyl-imidazole and benzothiazole substituted N, N-diethylamine rhodols were designed, synthesized and characterized. Their photophysical properties were studied in spirocyclic and open form from non-polar to polar solvents. The spirocyclic form exhibited larger Stokes shifts (50–260 nm) due to presence of ESIPT process whereas, open form showed small Stokes shift (10–40 nm) due to the lack of protons. Positive solvatochromism was observed for both the spirocyclic and open forms which is well supported by the linear (Lippert-Mataga and Mac-Rae) and multi-linear (Kamlet-Taft and Catalan parameters) analysis. Solvent polarizability (d_{SP}) is the major factor responsible for red shift in absorption/emission and larger Stokes shift for spirocyclic form. Polarity graphs and charge transfer descriptors are in good relation with Generalized Mulliken-Hush (GMH) parameters. From the solvatochromic data we observed that open forms show good TICT characteristics as compared to their respective spirocyclic forms. Open form is highly sensitive to viscosity as compared to spirocyclic form in a mixture of polar-protic solvents (EtOH:PEG 400). The experimental results are well correlated theoretically using Density Functional Theory (DFT) computations.

1. Introduction

Xanthene dyes such as rhodamine, fluorescein with reactive linker functionalities are extensively used in various applications as they are biocompatible, excite with low energy and emit with high fluorescence quantum yield [1–7]. The conformational changes in xanthenes (from spiro-lacton to open form) are useful in sensing the heavy metal ions [8–19]. The photophysical properties of xanthene derivatives can be altered by structural modifications using different synthetic strategies [20]. In addition, a new strategy to obtain red shifted absorption is reported where the xanthene oxygen is substituted by other atoms such as silicon and carbon [21,22].

Though xanthene derivatives are widely applied in numerous fields, they suffer a major drawback of small Stokes shift leading to self-quenching and errors in fluorescence detection [23,24]. Hence, a number of researchers in the past few years contributed to overcome the above drawbacks by synthesizing hybrid dyes such as ESIPT-BODIPY [25,26], ESIPT-coumarin [27,28], BODIPY-coumarin [29,30], BODIPY-rhodamine [31,32], and coumarin-rhodamine [33,34] with unique photophysical properties.

In the past few years, excited-state intramolecular proton transfer (ESIPT) in the molecules has emerged as a useful tool for sensing applications [35–40]. The ESIPT-active molecules give large Stokes shifts and change in fluorescence from excited enol and keto tautomers [41]. These properties of ESIPT molecules assist in designing numerous molecular probes for detection of targeted species [42–48]. 2-(2′-Hydroxyphenyl)-benzoxazole undergoes ESIPT process on photo-excitation in which rapid photo-induced proton transfer leads to tautomerization [49–51]. The blockage of ESIPT process in 2-(2′-hydroxyphenyl)-benzothiazole (HBT) mainly results in enol-like emission and is used as ratiometric sensing for the variety of analytes [52]. In the absence of analyte, the keto-form exhibits stronger fluorescence at longer wavelength on photo-excitation [53–62]. This unusual red shift in emission obtained with ESIPT molecules is useful for their applications in photochromic dyes [63], laser dyes [64], photo-stabilizers [65] and fluorescence recording techniques [66,67].

Rhodol is a hybrid form of fluorescein and rhodamine which shows excellent photophysical properties such as good solubility, photo- stability and high fluorescence quantum yield [68–71]. Rhodol has an acidic phenol moiety in their spirocyclic form that could be readily ionized to the more nucleophilic phenoxide ion in open form. This molecular configuration is the basis for the ESIPT process between the phenolic hydroxyl group and N-atom of the benzothiazole ring which exhibits similar emission properties like HBT [72,73]. This ESIPT process

---

* Corresponding author.
E-mail address: n.sekar@ictmumbai.edu.in (N. Sekar).

https://doi.org/10.1016/j.molliq.2019.111626

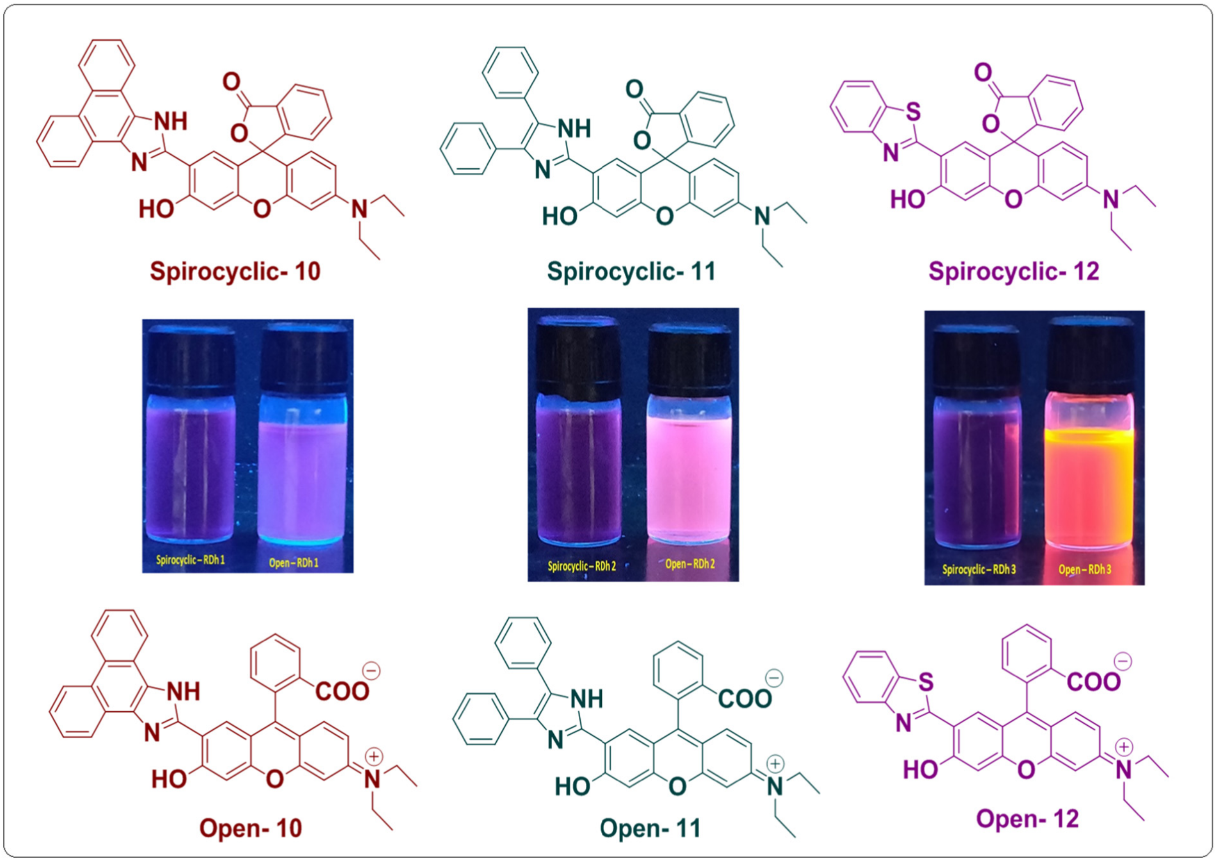

Fig. 1. Structures of the ESIPT-rhodol derivatives **10**, **11** and **12** (spirocyclic and open form) with their photographs under UV light in chloroform.

generates photo induced structural transformation of rhodols from phenol (enol) to keto form [74].

Herein, we report three rhodol derivatives **10**, **11**, and **12** (Fig. 1). In these compounds, benzimidazole and benzothiazole units were strategically introduced adjacent to oxygen atom of phenolic group of rhodol dyes. It is expected that the "phenol-quinone" transmission in these rhodol dyes switch the ESIPT process existing between the phenolic OH group and N atom of benzimidazole/benzothiazole ring in spirocyclic form. The ESIPT-rhodol derivatives were reported by Yang et al. as ratiometric probes for Cu^{2+} [75], Goswami et al. reported rhodol-based chemodosimeter for both Hg^{2+} and OCl^- [76], Zhang et al. reported rhodol-based far-red fluorescent probe for the detection of cysteine, homocysteine and glutathione [77] and the Strongin et al. rhodol-thioester fluorescent probe for the detection of glutathione and cysteine/homocysteine [78]. However, their photophysical properties in closed and open form, detailed solvatochromic properties, intramolecular-charge transfer (ICT) and twisted-intramolecular charge transfer (TICT), viscosity sensitivity and computational studies are not yet reported. Accordingly, herein we wish to report the solvatochromism of synthesized rhodols **10**, **11** and **12**, their relation with linear (i.e., Lippert-Mataga, Mac-Rae, Rettig's, and Generalized Mulliken-Hush polarity functions) and multilinear (i.e. Kamlet-Taft and Catalan equations) polarity functions, viscosity sensitivity in mixtures of polar-protic (EtOH:PEG 400) media. The observed experimental results correlated theoretically using Density Functional Theory (DFT) and Time Dependant-Density Functional Theory (TD-DFT).

2. Experimental

2.1. Materials and instruments

The required chemicals were purchased from the regional distributor, S. D Fine chemical limited, Mumbai, India. The samples were purified by using silica of 100–200 mesh size. ^1H and ^{13}C NMR spectra were recorded on 500 MHz and 100 MHz respectively on Agilent Technologies instrument (TMS as an internal standard). Perkin Elmer UV–visible spectrophotometer (Lambda 25) was used for absorption studies. Varian Cary Eclipse fluorescence spectrophotometer was used for emission studies. Melting points were recorded on melting point equipment from Sunder Industrial Products, Mumbai. Fluorescence quantum yield were calculated by using coumarin 6 ($\phi = 0.94$ in chloroform) and rhodamine 101 ($\phi = 0.94$in ethanol) as reference standards for spirocyclic and open form respectively.

2.2. Computational methods

DFT [79] computations of the synthesized rhodols were carried on Gaussian 09 [80] program using B3LYP hybrid functional. The B3LYP is combination of Becke's three exchange functional parameter (B3) [81] and the functional by Lee, Yang and Parr [82]. B3LYP/6-31 G (d) method was used for DFT and TD-DFT studies. Vertical excitation energies and oscillator strengths were obtained for lowest 10 singlet-singlet transitions at the optimized ground state equilibrium geometries by using TD-B3LYP/6-31 G (d) [83].

2.3. Synthesis and characterization

2-(4-(Diethyl amino)-2-hydroxybenzoyl) benzoic acid **2** was synthesized by using reported protocol [33]. 2,4-Dihydroxybenzaldehyde **4** was synthesized from resorcinol following the reported method [84]. Intermediate **4** was reacted with 9,10 phenanthrene-dione and benzil in a mixture of ammonium acetate and acetic acid to afford hydroxyl imidazole derivatives **5** and **7** respectively. Similarly, **4** was treated with 2-aminobenzenethiol **8** in sodium metabisulfite and DMF as solvent to afford 4-(benzo[*d*]thiazol-2-yl) benzene-1, 3-diol **9** in good yields (Scheme 1). All these intermediates **5**, **7** and **9** were reacted

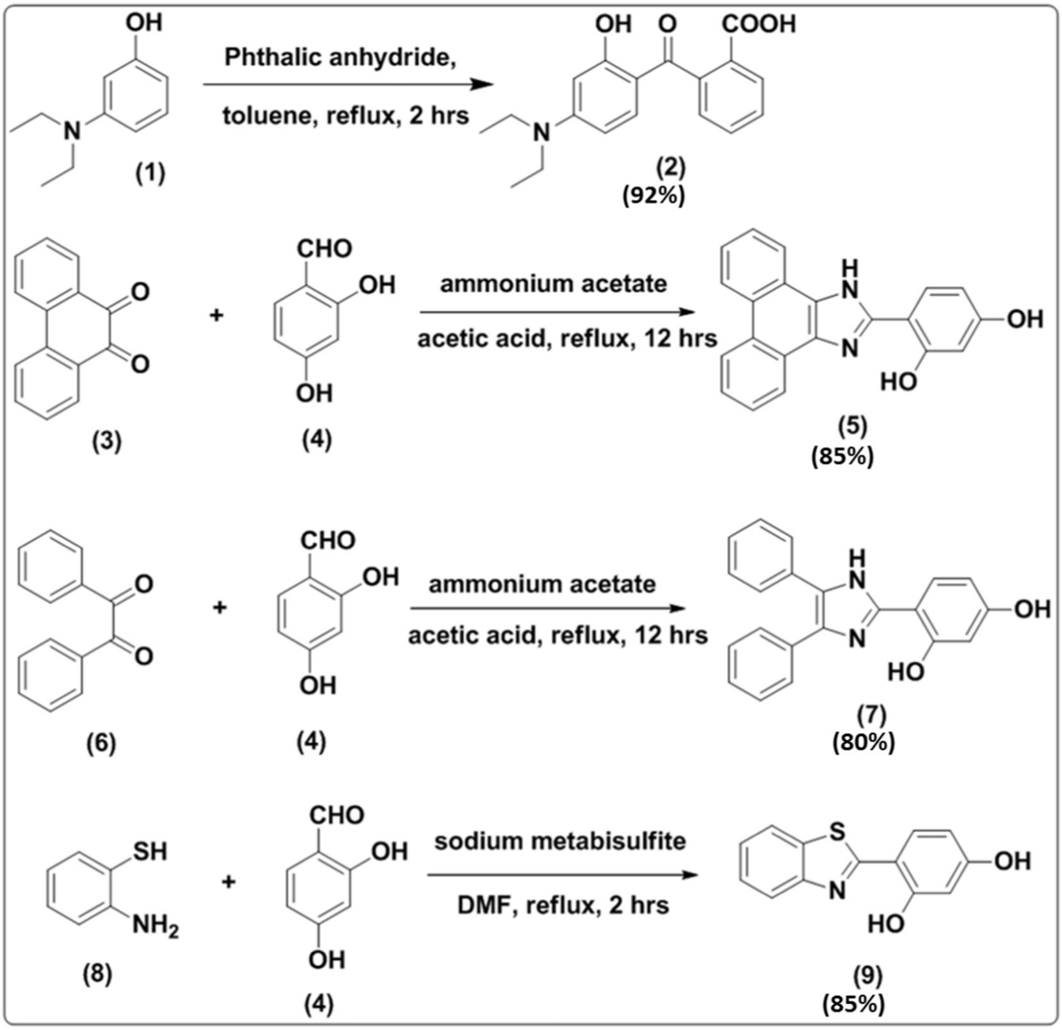

Scheme 1. Synthesis of phenanthrene-imidazole (**5**), diphenyl-imidazole (**7**) and thiazole-benzene (**9**) intermediates.

with N, N-diethyl meta amino phenol keto acid **2** in methane sulfonic acid to isolate respective ESIPT-rhodol derivatives **10**, **11** and **12** in their spirocyclic form and purified by column chromatography. The spirocyclic form of **10**, **11** and **12** were converted into their open form by the treatment of methanolic HCl (Scheme 2). The newly synthesized ESIPT-rhodol derivatives were fully characterized by ^{1}H, ^{13}C NMR, elemental and mass analysis.

*2.3.1. Synthesis of 4-(1H-phenanthro [9, 10-d] imidazol-2-yl) (**5**)*

The compound **5** was synthesized according to the reported method [85]. 2, 4-Dihydroxy benzaldehyde (0.12 g, 0.72 mmol) was reacted with phenanthre-9, 10-dione (0.13 g, 0.624 mmol) and ammonium acetate (0.86 g, 11.20 mmol) in acetic acid (10 ml). The reaction mixture was refluxed for 4–5 h. On completion of the reaction, the reaction mass was cooled to room temperature and quenched with water. The reaction mixture was then neutralized with aq. ammonia solution. During the neutralization process the solid precipitated out, which was filtered and washed with water and dried under vacuum. The purification of crude product was done by column chromatography (eluent system; ethyl acetate in hexane 10–30%) to obtain white colored pure product (0.170 g, 85%) (Scheme 1).

*2.3.2. Synthesis of 4-(4, 5-diphenyl-1H-imidazolyl)-benzene-1, 3-diol (**7**)*

Compound **7** was synthesized according to the reported method [86]. 2, 4-Dihydroxy benzaldehyde **4** (0.1 g, 0.724 mmol) was reacted with ammonium acetate (0.88 g, 11.4 mmol) and benzil **6** (0.13 g, 0.618 mmol) in acetic acid (10 ml). The reaction mixture was refluxed for 4–5 h. On completion of the reaction, the reaction mass was cooled to room temperature and quenched with water. The reaction mixture was then neutralized with aq. ammonia. During the neutralization process the solid precipitated out, which was filtered and washed with water. The crude product obtained was purified by column chromatography using 10–30% ethyl acetate in hexane to obtain the pure product as white solid (0.160 g, 80%) (Scheme 1).

*2.3.3. Synthesis of 4-(benzo[d] thiazole-2-yl)-benzene-1, 3-diol (**9**) [87]*

2-Amino thiophenol **8** (0.33 ml, 3.12 mmol), sodium metabisulfite ($Na_2S_2O_5$, 0.610 g) and 2, 4-dihydroxy benzaldehyde **4** (0.446 g, 3.18 mmol) were refluxed in dry DMF (20 ml) for 2 h. The reaction mixture was cooled to room temperature and water (200 ml) was added slowly to the reaction mixture. After completion of the addition, the solid precipitated out which was filtered, washed with water (60 ml) and dried to yield crude product. The crude product was purified by recrystallization from methanol to obtain light yellow solid product (0.634 g, 85%) (Scheme 1).

*2.4. Synthesis of rhodol derivatives (**10**, **11** and **12**)*

Compound **10** was obtained by refluxing **5** (0.101 g, 0.307 mmol) with **2** (0.128 g, 0.41 mmol) in methanesulfonic acid (5 ml). Compound **11** was obtained by refluxing **7** (0.101 g, 0.305 mmol) with **2** (0.128 g, 0.41 mmol) in methanesulfonic acid (5 ml). Compound **12** was obtained

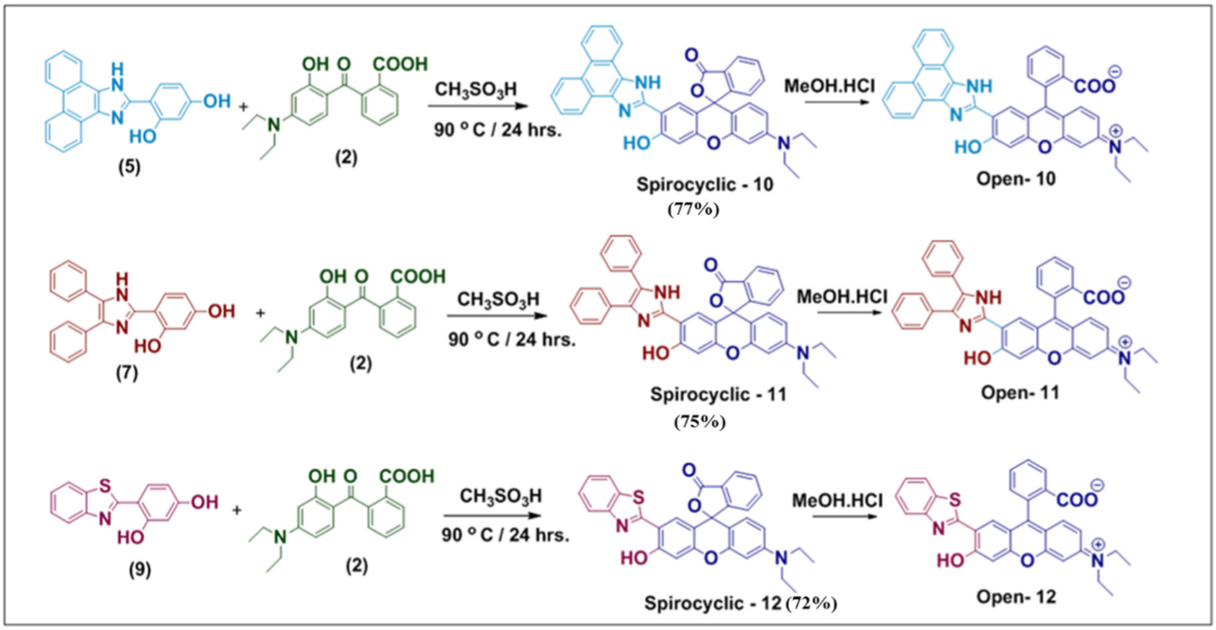

Scheme 2. Synthesis of ESIPT-rhodol derivatives (**10**, **11** and **12**).

on refluxing **9** (0.100 g, 0.41 mmol) with **2** (0.128 g, 0.41 mmol) in methanesulfonic acid (5 ml). The temperature of the reaction mixture was maintained at 90–95 °C for 24 h (Scheme 2). Then, reaction mass was cooled to room temperature and poured in ice-water (30 ml). After sometime the precipitated product was washed three times with brine water solution (3 × 5 ml) and then dried under vacuum to give the crude product. The purification was done by column chromatography using 1–2% methanol in chloroform as an eluent system to afford solid product.

2.4.1. Characterization (**10**, **11** and **12**)

*2.4.1.1. 6′-(Diethyl amino)-3′-hydroxy-2′-(1H-phenanthro [9, 10-d] imidazol-2-yl)-3H-spiro [isobenzofuran-1, 9′-xanthen]-3-one (**10**).* Yield: 77%, melting point: 289 °C, ^{1}H NMR (400 MHz, DMSO) δ 13.75 (s, 1H), 8.80 (d, *J* = 6.7 Hz, 2H), 8.36 (s, 3H), 8.09 (d, *J* = 7.1 Hz, 1H), 7.81–7.67 (m, 5H), 7.62 (d, *J* = 7.4 Hz, 2H), 7.30 (d, *J* = 6.6 Hz, 1H), 6.97 (s, 1H), 6.45 (d, *J* = 12.5 Hz, 3H), 1.06 (t, *J* = 6.5 Hz, 6H). ^{13}C NMR (101 MHz, DMSO) δ 169.62, 159.98, 153.28, 152.10, 149.65, 148.74, 136.11, 136.10, 130.51, 128.78, 126.45, 125.44, 125.43, 124.45, 122.80, 122.07, 111.42, 111.04, 109.29, 109.27, 105.37, 104.35, 97.37, 44.22, 12.74. Mass analysis: Calculated for ($C_{39}H_{29}N_3O_4$): 603.2, found: 604.1 (M+1). Elemental analysis ($C_{39}H_{29}N_3O_4$): Calculated: C – 77.60, H – 4.84, N – 6.96. Found: C – 77.63, H – 4.84, N – 6.97.

*2.4.1.2. 6′-(Diethyl amino)-2′-(4, 5-diphenyl-1H-imidazol-2-yl)-3′-hydroxy-3H-spiro [isobenzofuran-1, 9′-xanthen]-3-one (**11**).* Yield: 75%, melting point: 272 °C, ^{1}H NMR (400 MHz, DMSO) δ 13.76 (s, 1H), 7.99 (d, *J* = 7.1 Hz, 2H), 7.70 (dd, *J* = 18.4, 6.8 Hz, 2H), 7.55 (s, 1H), 7.39 (m, 7H), 7.23 (dd, *J* = 56.0, 7.2 Hz, 4H), 6.86 (s, 1H), 6.46–6.36 (m, 3H), 1.05 (t, *J* = 6.8 Hz, 6H). ^{13}C NMR (101 MHz, DMSO) δ 169.55, 159.22, 153.59, 153.58, 152.47, 152.04, 149.55, 145.19, 145.17, 135.93, 135.91, 135.90, 135.87, 130.31, 130.28, 130.27, 129.27, 128.97, 128.82, 126.36, 125.46, 125.21, 125.20, 124.31, 110.98, 109.18, 105.28, 103.97, 97.31, 44.20, 12.74. Mass analysis: Calculated for ($C_{39}H_{31}N_3O_4$): 605.23, found: 606.1 (M+1). Elemental analysis ($C_{39}H_{31}N_3O_4$): Calculated: C – 77.68, H – 4.47, N – 6.91. Found: C – 77.66, H – 4.46, N – 6.92.

*2.4.1.3. 2′-(Benzo[d]thiazol-2-yl)-6′-(diethylamino)-3′-hydroxy-3H-spiro [isobenzofuran-1, 9′-xanthen]-3-one (**12**).* Yield: 72%, melting point: 255 °C, ^{1}H NMR (400 MHz, DMSO) δ 13.76 (s, 1H), 9.01 (s, d = 8.6 Hz, 2H), 8.00 (d, *J* = 8.6 Hz, 2H), 7.82 (s,1H), 7.37 (m, 3H), 7.13 (d, *J* = 5.3 Hz, 2H), 6.58 (d, *J* = 6.5 Hz, 2H), 6.41 (s, 1H), 1.19 (t, *J* = 7.1 Hz, 6H), ^{13}C NMR (126 MHz, DMSO) δ 166.93, 161.23, 155.77, 151.35, 135.57, 133.96, 131.90, 131.24, 130.71, 130.70, 129.67, 129.29, 126.86, 125.57, 122.81, 122.36, 120.39, 120.31, 117.07, 116.98, 116.56, 114.80, 103.74, 97.72, 84.30, 46.63, 12.98. Mass analysis: Calculated for ($C_{31}H_{24}N_2O_4S$): 520.1, found: 521.1 (M+1). Elemental analysis ($C_{31}H_{24}N_2O_4S$): Calculated: C – 77.51, H – 4.65, N – 6.16. Found: C – 77.54, H – 4.64, N – 6.17.

3. Results and discussion

3.1. Photophysical properties

Absorption and emission spectra of ESIPT-rhodols were investigated in both spirocyclic as well as open forms in seven organic solvents of different polarities. The spirocyclic forms **10**, **11** and **12** are colorless while in open form they are shiny reddish black colored solids. The spirocyclic form of rhodols on treatment with methanolic HCl solution transform into open form-rhodols. After repeating twice the above procedures, the solvent was evaporated on rotary evaporator to get open form of **10**, **11** and **12** as shiny reddish black solids. Due to the ESIPT process, spirocyclic-rhodols **10**, **11** and **12** show larger Stokes shift (50–260 nm) than the open form-rhodols **10**, **11** and **12** (10–40 nm). Fig. 2 shows the absorption and emission spectra of spirocyclic and open form of **10**, **11** and **12** in chloroform. In spirocyclic form, rhodol **10** show red shifted absorption as compared to **11** and **12**, but the opposite trend is observed in emission and Stokes shifts. The compounds **11** and **12** show red shifted emission and large Stokes shift as compared to **10**. All spirocyclic forms absorbed in the range of 330–370 nm in chloroform. Spirocyclic **10** emits at 428 nm while, spirocyclic **11** and **12** emit at 445 nm and 525 nm respectively in chloroform while the open form **10** shows highly red shifted emission at 610 nm compared to open forms **11** and **12**. All the compounds in open form absorb at 335–340 nm and emit at 590–600 nm in chloroform. In their spirocyclic form molar extinction coefficients were higher in comparison with their open forms. From the experimental results for spirocyclic and open forms, the oscillator strength (f) and transition dipole moment (μ_{eg}) were calculated by using reported expressions [88]. In addition, the ESIPT-

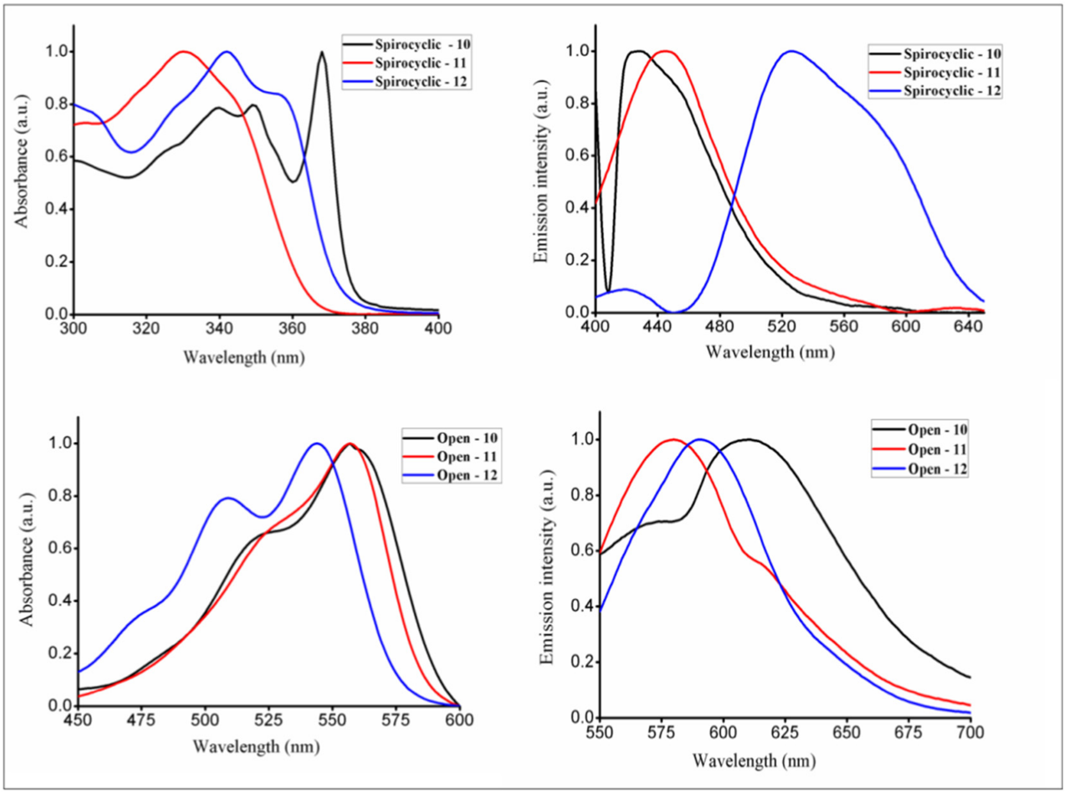

Fig. 2. Normalized absorption and emission spectra of compound **10**, **11** and **12** in spirocyclic form and open form in chloroform.

rhodols show higher transition dipole moment and oscillator strength in open form in comparison with their spirocyclic form (Table 1).

Complete photophysical parameters of dye **10** in their spirocyclic form and open form are presented in Tables 2 and 3.

3.2. Solvatochromism

From Tables S1–S6 it was observed that ESIPT-rhodol derivatives **10**, **11** and **12** in spirocyclic form shows red shift in absorption and emission spectra as we go from non-polar solvents to polar solvents suggesting that highly polar excited state in polar solvents [89,90]. Fig. 3 represents the normalized absorption and emission spectra of spirocyclic **12** which shows a red shift in absorption and emission spectra in non–polar to polar solvents. Interestingly, in their open form **10**, **11** and **12** show intense red shift from non-polar to polar solvents in the absorption and slightly red shift in emission. Fig. 4 shows normalized absorption and emission spectra of the open form of **12**.

Red shifted absorption and emission in solvents of different polarity are mainly due to the fact that the excited state of the compounds is influenced by the dipole-dipole interaction, and solute-solvent interaction. To correlate the effect of refractive index and dielectric constant of solvents on emission λ_{max} values with the observed solvatochromism in dyes we used Lippert-Mataga and Mac-Rae equations [91–93]. The observed linear relationship between the Stokes shift and Lippert-Mataga function, Mac-Rae function for the dyes in their spirocyclic and open forms (Fig. 5) suggests that refractive index and dielectric constant are together responsible for red shift in emission in polar solvents.

3.3. Generalized Mulliken Hush (GMH) analysis of intramolecular charge transfer (ICT)

The strength of electronic intramolecular charge transfer (ICT) in the dyes, can be measured to predict the solvatochromism in dyes, as greater charge transfer leads to highly polar excited state resulting in positive solvatochromism. The equation for two-state GMH analysis of ICT in molecules is presented as [94],

$$\Delta\mu_{ab}^2 = \Delta\mu_{ge}^2 + 4\mu_{ge}^2 \tag{1}$$

The, $\Delta\mu_{ge}^2$ and μ_{ge}^2 terms are obtained from Lippert-Mataga equation and absorption plots respectively. The electronic coupling between the

Table 1
Photophysical properties of compound **10**, **11** and **12** for both forms in chloroform solvent.

Compounds	λ_{abs} (nm)	$\varepsilon_{max} \times 10^4$ (M^{-1} cm^{-1})	FWHM (nm)	λ_{ems} (nm)	Stokes shift (nm)	Stokes shift (cm^{-1})	ϕ_f	f	μ_{eg} (debye)
10 (spirocyclic)	368	7.86	72	428	60	3800	0.154	0.19	3.79
11 (spirocyclic)	330	4.96	53	445	115	7800	0.152	0.88	7.89
12 (spirocyclic)	342	5.46	64	525	183	10,200	0.157	0.91	8.16
10 (open)	556	2.8	89	610	54	1600	0.321	3.42	19.76
11 (open)	557	1.54	85	578	21	650	0.314	3.01	18.48
12 (open)	544	2.91	66	590	46	1400	0.329	3.32	19.55

λ_{abs} – absorption maximum wavelength. λ_{emm} – emission maximum wavelength. ε_{max} – molar extinction coefficient. FWHM – full width half wave maxima. ϕ_f – Fluorescence quantum yield. *f* – Oscillator strength. μ – transition dipole moment.

Table 2
Photophysical properties of **10** in their spirocyclic form in all solvents.

Solvent	λ_{abs} (nm)	$\varepsilon_{max} \times 10^4$ (M^{-1} cm^{-1})	FWHM (nm)	λ_{ems} (nm)	Stokes shift		ϕ_f	f	μ_{eg} (debye)
					(nm)	(cm^{-1})			
Hexane	366	9.39	74	416	50	3200	0.086	0.18	3.79
Toluene	367	3.77	75	428	61	3900	0.132	0.68	7.33
$CHCl_3$	368	7.86	72	428	60	3800	0.154	0.19	3.79
EA	369	3.22	71	438	69	4300	0.144	0.58	6.72
MeOH	369	1.74	71	451	82	4900	0.095	0.22	4.12
Dioxane	371	2.86	73	454	83	4900	0.327	0.55	6.59
DMSO	371	3.08	75	459	88	5200	0.347	0.61	6.95

Table 3
Photophysical properties of **10** in their open form in all solvents.

Solvent	λ_{abs} (nm)	$\varepsilon_{max} \times 10^4$ (M^{-1} cm^{-1})	FWHM (nm)	λ_{ems} (nm)	Stokes shift		ϕ_f	f	μ_{eg} (debye)
					(nm)	(cm^{-1})			
Hexane	536	7.3	141	598	62	1900	0.135	1.01	10.86
Toluene	546	1.53	93	602	56	1700	0.26	1.82	14.82
$CHCl_3$	556	2.8	89	610	54	1600	0.321	3.42	19.76
EA	565	6.68	82	618	53	1500	0.292	0.59	8.48
MeOH	566	1.96	75	614	48	1400	0.157	2.09	15.75
Dioxane	566	1.38	68	618	52	1500	0.592	1.14	11.72
DMSO	567	2.45	89	623	56	1600	0.647	0.21	4.93

donor (D) and acceptor (A) group is an important factor in controlling the charge transfer for D-π-A system [95]. Hence it is essential to estimate the D-π-A coupling matrix value (H_{ab}) to better understand the behaviour of long- distance charge transfer, where, 'a' and 'b' are initial and final diabatic states, which are characterized as the ground and excited states in charge transfer process. The coupling matrix in adiabatic states of D-π-A system can be denoted as H_{DA}, and are assumed to be composed of three diabatic states (i.e. donor group state (GS), donor locally excited state (ES) and charge transfer state (CT) transferring charge from donor to the acceptor unit). The degree of delocalization (C_b^2) and donor-acceptor coupling matrix value (H_{DA}) calculated from spectroscopic data for **10**, **11**, and **12** in their spirocyclic as well as open form by using following equation,

$$C_b^2 = \frac{1}{2}\left(1 - \sqrt{\frac{\Delta\mu_{ge}^2}{\Delta\mu_{ge}^2 + 4\mu_{ge}^2}}\right) \tag{2}$$

$$H_{DA} = \frac{\Delta E_{ge}\mu_{ge}}{\Delta\mu_{ge}^D} \tag{3}$$

Within the two-level approximation in Eq. (3), (H_{DA}) is correlated with the vertical excitation energy (ΔE_{ge}), the difference between the adiabatic dipole moments of the ground and excited states ($\Delta\mu_{ge}$). The difference in diabatic state dipole moments and the transition dipole moments ($\Delta\mu_{ge}^D$) is correlated by GMH method [95,96] as follows,

$$H_{DA} = \frac{\Delta E_{ge}\mu_{ge}}{\Delta\mu_{ge}^D} = \frac{\Delta E_{ge}\cdot\mu_{ge}}{\sqrt{\Delta\mu_{ge}^2 + 4\mu_{ge}^2}} \tag{4}$$

The charge transfer D-π-A coupling distance (R_{DA}) [96] can be determined by using Eq. (5),

$$R_{DA} = 2.06 \times 10^{-2}\frac{\sqrt{\Delta E_{ge}\varepsilon_{max}\Delta\nu_{1/2}}}{H_{DA}} \tag{5}$$

where, 'ε_{max}' and '$\Delta\upsilon_{1/2}$' are the molar absorptivity ($L\cdot M^{-1}\cdot cm^{-1}$) and bandwidth ($cm^{-1}$) respectively.

The observed results of GMH analysis show that there is a good charge transfer in spirocyclic and open form of **10**, **11** and **12** as degree of delocalization (C^2b) and D-π-A coupling value (H_{DA}) increases with solvent polarity. Similarly **10**, **11** and **12** showed positive solvatochromism as D-π-A coupling distance (R_{DA}) values decreased with solvent polarity for **10**, **11** and **12** in their spirocyclic as well as open form (Tables 4 and 5).

3.4. Multi-linear regression analysis using Kamlet-Taft and Catalan equations

In general linear correlation parameters such as Lippert-Mataga and Mac-Rae polarity functions are used to understand the effect of solvent polarity on observed absorption and emission shift, but these parameters are not explaining precisely which solvent parameters such as solvent acidity, basicity, dipolarity or polarizability are responsible for observed spectral shift. Hence multilinear approach is proposed by Kamlet and Taft [97,98] as represented in Eq. (6)

$$y = y_0 + a_\alpha\alpha + b_\beta\beta + c_{\pi^*}\pi^* \tag{6}$$

where, 'y' is solvent affected physiochemical property (e.g. absorption maxima ($\overline{\upsilon}_{abs}$), emission maxima ($\overline{\upsilon}_{emm}$) and Stokes shift ($\Delta\upsilon$) etc.). '$y_0$' is studied physiochemical property in gas phase, while a, b, c, and d are adjustable coefficients which reflect the dependence of 'y' to the various solvent parameters (e.g. effect of solvent acidity (α), effect of solvent basicity (β), collective effect of solvent polarity/dipolarity as well as solvent polarizability (π^*) etc.). However, if solvent acidity and basicity are not affecting the value of 'y', then among solvent polarity, dipolarity and polarizability it is difficult to find out which factor is exactly influencing the studied physiochemical property

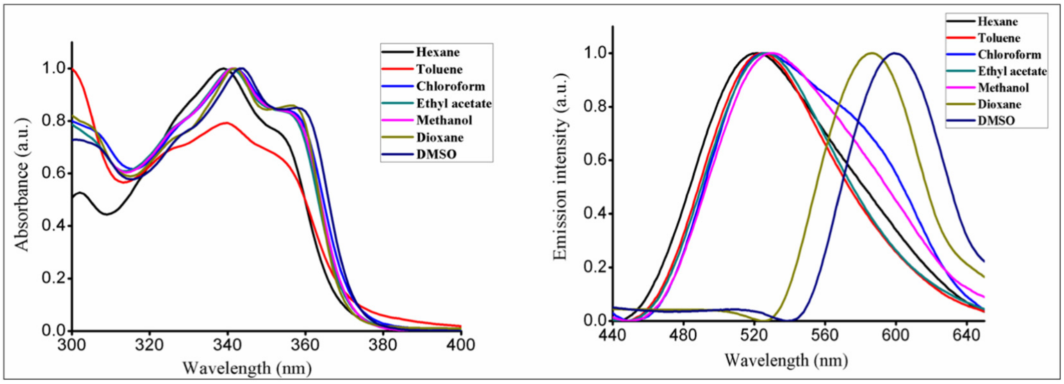

Fig. 3. Absorption and emission spectra of spirocyclic **12**.

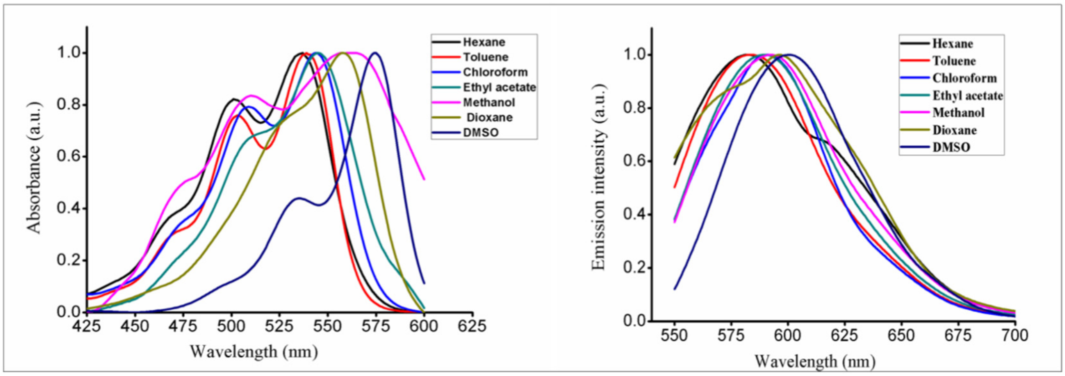

Fig. 4. Absorption and emission spectra of open **12**.

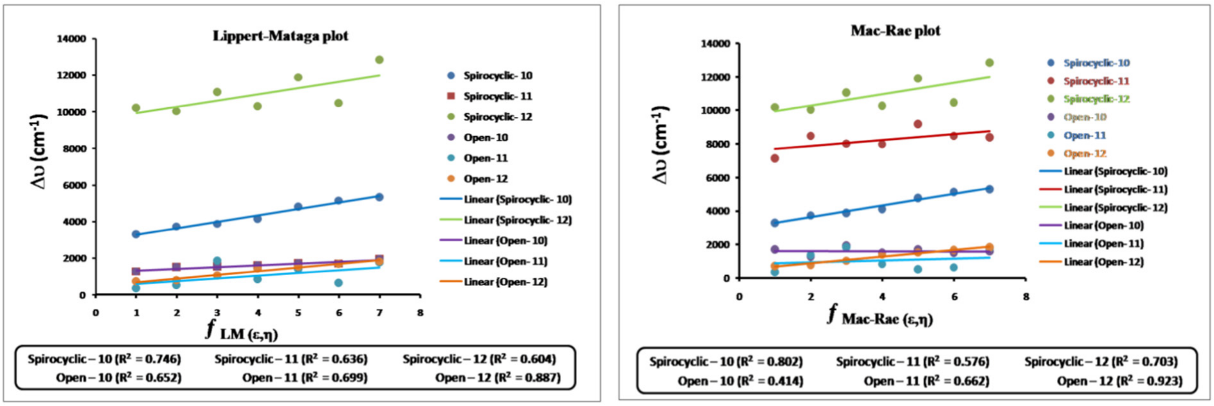

Fig. 5. Lippert-Mataga and Mac-Rae plots for compound **10**, **11** and **12**.

'y', hence Catalan [99–101] introduced another expression as represented in Eq. (7)

$$y = y_0 + a_{SA}\mathrm{SA} + b_{SB}\mathrm{SB} + c_{SP}\mathrm{SP} + d_{SdP}\ \mathrm{SdP} \qquad (7)$$

where, Catalan used same solvent parameters (e.g. solvent acidity (SA), solvent basicity (SB) etc.), which is already utilized by Kamlet and Taft. Here, he divided the last parameter 'π^*' into two separate parameters such as solvent polarizability (SP) and solvent dipolarity (SdP). The Catalan parameters are modified version of Kamlet-Taft parameters, here we used both the parameters simultaneously to understands the exactly which factor is influence the observed spectral shift in absorption and emission spectra from non-polar to polar solvents in all dyes **10**, **11**, and **12**. Taft and Kamlet [102] and Catalán [103] functions are used to find out the main factor influence the absorption spectra, emission spectra and the Stokes shifts in solvents of various polarity. The positive value for various factors in multi-linear analysis method indicates the negative solvatochromism, whereas, the negative values for factors in multi-linear analysis methods indicate positive solvatochromism. The details of analysis employing Kamlet-Taft (Eq. (6)) and Catalan (Eq. (7)) parameters together for multi-linear analysis of ν_{abs} (absorption maxima), ν_{emn} (emission maxima) and $\Delta\nu$ (the Stokes shift) for spirocyclic **10** in seven solvents of various polarity are shown in Table 6.

Catalan parameters (0.86, 0.97, and 0.71) show higher values for absorption maxima ($\overline{\upsilon}_{abs}$), emission maxima ($\overline{\upsilon}_{emi}$) and Stokes shift ($\Delta\overline{\upsilon}$) respectively than Kamlet-Taft parameters (0.54, 0.87, and 0.21). From Table 6 it is clear that solvent polarizability factor (d_{SP}) is the major factor responsible for red shift in absorption and emission spectra of spirocyclic **10**.

Tables S7–S12 show multi-linear analysis in solvents of different polarity by using Kamlet-Taft and Catalan parameters together for **10**, **11** and **12** in spirocyclic and open form. Similarly, for spirocyclic **11** and **12**, solvent polarizability (d_{SP}) mainly responsible for red shift in

Table 4
Degree of delocalization (C^2b), donor-acceptor coupling value (H_{DA}) and donor-acceptor coupling distance (R_{DA}) values for spirocyclic form **10**, **11** and **12**.

Solvent	Spirocyclic - **10**			Spirocyclic - **11**			Spirocyclic - **12**		
	C^2b	H_{DA} (cm^{-1})	R_{DA} (Å)	C^2b	H_{DA} (cm^{-1})	R_{DA} (Å)	C^2b	H_{DA} (cm^{-1})	R_{DA} (Å)
Hexane	0.4906	13,476.3	28.1	0.486	15,059.7	33.2	0.4921	14,490.9	34.9
Toluene	0.4909	13,476.4	26	0.495	15,151.2	25.5	0.4961	14,577	30.6
$CHCl_3$	0.4911	13,547.7	16.8	0.4961	15,243.4	21.9	0.496	14,619.5	22.4
EA	0.4944	13,549.2	17.7	0.4959	15,237.9	22.9	0.4967	14,662.6	22.7
MeOH	0.4946	13,586.1	12.3	0.4963	15,290	17.7	0.4963	14,619.4	21.7
Dioxane	0.4948	13,621.8	15.6	0.4955	15,243.2	21.9	0.4978	14,662.3	22.2
DMSO	0.4951	13,658.9	16	0.497	15,575.5	15.3	0.4976	14,748.7	11.4

Table 5
Degree of delocalization (C^2b), donor-acceptor coupling value (H_{DA}) and donor-acceptor coupling distance (R_{DA}) values for open form **10**, **11** and **12**.

Solvent	Open - **10**			Open - **11**			Open - **12**		
	C^2b	H_{DA} (cm^{-1})	R_{DA} (Å)	C^2b	H_{DA} (cm^{-1})	R_{DA} (Å)	C^2b	H_{DA} (cm^{-1})	R_{DA} (Å)
Hexane	0.4933	8817.5	53.5	0.4734	8805.9	60.4	0.4841	8710.6	63.4
Toluene	0.4976	8833.8	39.7	0.4935	8896	57	0.4926	8976.3	60.1
$CHCL_3$	0.4968	8833.7	49.6	0.4935	8960	39.9	0.4956	9190.9	43.7
EA	0.4978	8992.7	44	0.4943	8975.9	40.5	0.4964	8959.6	50.4
MeOH	0.497	8849.2	21.9	0.4977	9345.7	28.1	0.4983	9276.4	15.6
Dioxane	0.4959	9157.3	27.9	0.4982	8976.6	35.5	0.4968	9169.7	28.8
DMSO	0.4982	9328.3	16.2	0.4982	9363.2	13.3	0.4983	9310.9	15.9

Table 6
Multi-linear analysis of ($\overline{\upsilon}_{abs}$), ($\overline{\upsilon}_{emi}$) and ($\Delta\overline{\upsilon}$) of compound spirocyclic **10** by using Kamlet-Taft and Catalan parameters.

Kamlet-Taft	$y_0 \times 10^3$	a_α	b_β	$c_{\pi *}$	r
$\overline{\upsilon}_{abs}$	18.08 ± 0.32	0.59 ± 0.48	−1.32 ± 0.75	0.41 ± 0.62	0.54
$\overline{\upsilon}_{emi}$	16.53 ± 0.11	0.31 ± 0.16	−1.0 ± 0.25	0.21 ± 0.21	0.87
$\Delta\overline{\upsilon}$	1.55 ± 0.22	0.27 ± 0.33	−0.33 ± 0.51	0.21 ± 0.43	0.21

Catalan	$y_0 \times 10^3$	a_{SA}	b_{SB}	c_{SdP}	d_{SP}	r
$\overline{\upsilon}_{abs}$	19.00 ± 1.03	−0.43 ± 0.71	−2.34 ± 0.69	3.36 ± 1.33	−3.87 ± 2.00	0.86
$\overline{\upsilon}_{emi}$	16.92 ± 0.28	−0.13 ± 0.19	−1.45 ± 0.19	−1.32 ± 0.37	−1.48 ± 0.55	0.97
$\Delta\overline{\upsilon}$	2.08 ± 0.78	−0.31 ± 0.54	−0.90 ± 0.52	2.04 ± 1.01	−2.39 ± 1.52	0.71

absorption and emission spectra, whereas, solvent polarizability (d_{SP}) is the main factor responsible for observed Stokes shift in spirocyclic **10**, **11** and **12**.

The graph plotted for the predicted emission data collected by Kamlet-Taft and Catalan parameters with the experimental data for all the compounds showed remarkable linear fit with the regression of 0.97, 0.73, and 0.95 for spirocyclic form **10**, **11** and **12** respectively whereas,0.99, 0.88, 0.82 for open form **10**, **11** and **12** (Fig. 6).

3.5. Twisted intramolecular charge transfer (TICT) characteristics

As there is a possibility of rotation between the benzimidazole and benzothiazole on one part and N,N- diethyl amine substituent on another part of compound **10**, **11** and **12** in their spirocyclic as well as open form, we studied the TICT characteristics of these compounds. In addition, the free rotating phenyl group at xanthene core suggests the possibility of twisted intramolecular charge transfer (TICT) characteristic in both spirocyclic as well as in open form. The TICT characteristics of

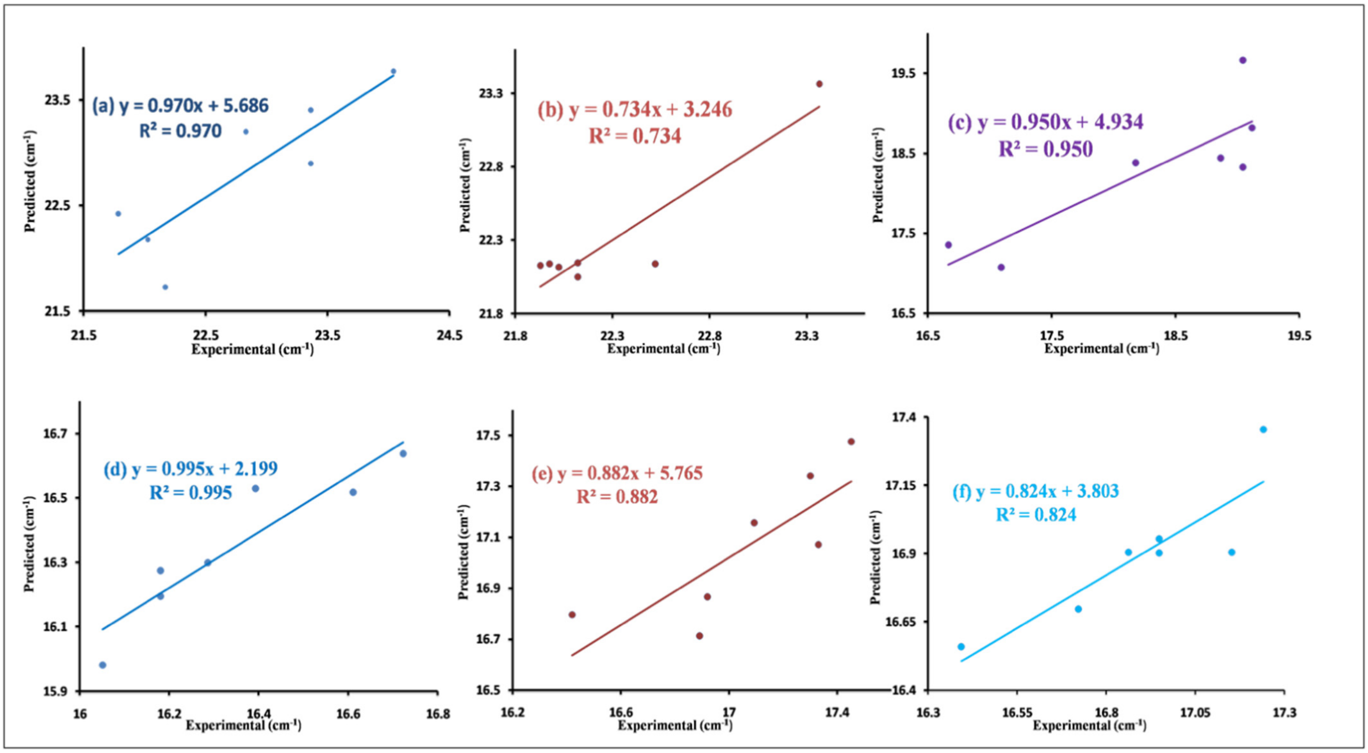

Fig. 6. Correlation between experimental and predicted emission wave numbers for spirocyclic - (a) **10**, (b) **11**, (c) **12** and open- (d) **10**, (e) **11** and (f) **12** by multi-linear analysis method.

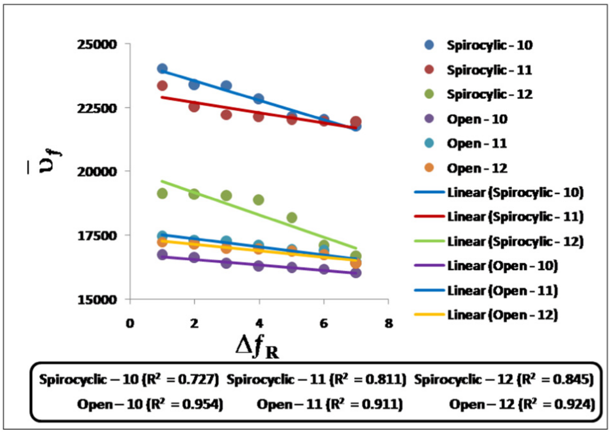

Fig. 7. Rettig's plot for spirocyclic as well as open form - **10**, **11** and **12**.

10, **11** and **12** were investigated by using Rettig's [104] Eq. (8)

$$\bar{\upsilon}_f = \frac{2\mu_e^2}{hca^3}\Delta f_R + C \qquad (8)$$

Here $\bar{\upsilon}_f$, c, a, C and μ_e are emission, velocity of light, Onsager radii, constant and dipole moment in excited state respectively. 'Δf_R' is Rettig's polarizability orientation which correlated with the emission wave number ($\bar{\upsilon}_f$) in Eq. (9),

$$\Delta f_R = \left[\frac{\varepsilon-1}{\varepsilon+2} - \frac{\eta^2-1}{2\eta^2+4}\right] \qquad (9)$$

Herein, we observed linear relation in **10**, **11** and **12** from non–polar to polar solvents with the Rettig's function (Fig. 7) with regression values for the dyes 0.727, 0.811 and 0.845 for spirocyclic form **10**, **11** and **12** respectively. Similarly 0.954, 0.911 and 0.924 for open form **10**, **11** and **12** respectively.

From above results it is seen that **10**, **11** and **12** exhibit TICT in the molecule from substituents such as benzimidazole and benzothiazole on one part and N, N-diethyl amine on the other part in their spirocyclic form.

3.6. Viscosity sensitivity of spirocyclic and open form rhodols

From Rettig's plot we concluded that **10**, **11** and **12** show TICT characteristics in their both spirocyclic and open form. To correlate these experimental results, we examined the viscosity sensitivity of these ESIPT-rhodol derivatives in ethanol: PEG 400 mixture. The possible intramolecular rotation of donor and acceptor substituents around single bond can be restricted by the rigidification of chemical structures [84,105]. In case of rhodols **10**, **11** and **12** there are possibilities of rotation for benzimidazole and benzothiazole substituents on one side and N,N–diethyl amine on the another side and the free rotating phenyl group on middle xanthene part. So, we were interested in the fluorescent molecular rotors (FMR) properties of these dyes.

For the viscosity sensitivity study we prepared 10 μM sample solutions in ethanol, by increasing the percentage of polyethylene glycol (PEG 400) from 0 to 100% in ethanol sample solution. Compounds **10**, **11** and **12** were investigated for viscosity sensitivity in their both spirocyclic and open form. Both the forms show enhancement in emission intensity with the increase in percentage of polyethylene glycol (PEG 400) in ethanol. Interestingly, we observed very good enhancement in emission intensity for open form of **10**, **11** and **12** as compared to their spirocyclic form. Hence, it can be concluded that the availability of free rotating phenyl group at xanthene core in the open form is mainly responsible for highly sensitivity to the viscous medium. Fig. 8 shows the availability of free rotating phenyl ring in the open form compared to the spirocyclic form. Two possible rotating sites are present in the spirocyclic form of **10**, **11** and **12** whereas, in the open form of **10**, **11** and **12** there are three possible rotating sites.

We observed 4.8, 4 and 6 fold enhancement in emission intensity for the spirocyclic form of **10**, **11** and **12** while 12.41, 33.44 and 7.09 fold enhancement in emission intensity for the open forms of **10**, **11** and **12**

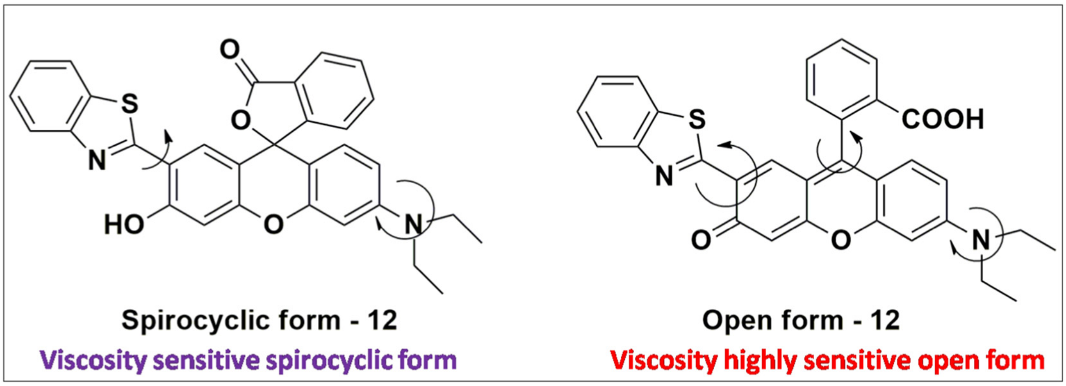

Fig. 8. Open form (highly viscosity sensitive) and spirocyclic form (viscosity sensitive) of compound **12**.

Table 7
Photophysical data for **10**, **11** and **12** in ethanol and (2:98) ethanol:PEG 400.

Compound	λ_{abs} (EtOH)	λ_{emm}(EtOH)	λ_{abs} (98%PEG 400)	λ_{emm} (98% PEG 400)	$\phi^{(\alpha)}$	$\phi^{(b)}$	x	R^2
Spirocyclic - **10**	372	438	377	450	0.115	0.552	0.091	0.822
Spirocyclic - **11**	338	435	349	436	0.127	0.611	0.093	0.906
Spirocyclic - **12**	352	589	358	600	0.147	0.706	0.061	0.876
Open - **10**	545	602	552	599	0.172	0.826	0.229	0.993
Open - **11**	562	585	569	616	0.185	0.742	0.26	0.953
Open - **12**	542	592	551	599	0.197	0.788	0.24	0.976

ϕ^a – Fluorescence quantum yield for compound in ethanol. ϕ^b – Fluorescence quantum yield for compound in 98% PEG 400.

respectively. The viscosity sensitivity data for **10**, **11** and **12** in their both spirocyclic and open form are shown in Table 7.

The synthesized rhodol derivatives show viscosity sensitivity in order of **11** > **10** > **12** in spirocyclic form whereas, open form follow the viscosity sensitivity order as **11** > **12** > **10** (Fig. 9).

The relation between the viscosity of solvent mixture and change in emission intensity is illustrated by using Forster-Hoffmann Eq. (10).

$$\log I = C + x \ \log \eta \tag{10}$$

In the above equation, I, C, x and η are the maximum emission intensity, constant, viscosity sensitivity parameter and viscosity of solvent system respectively. The 'x' values of 0.091 ($R^2 = 0.822$), 0.093 ($R^2 = 0.906$) and 0.061 ($R^2 = 0.876$) were observed for spirocyclic form **10**, **11** and **12** respectively (Fig. 10). Similarly, viscosity sensitivity parameter for the open forms **10**, **11** and **12** were 0.229 ($R^2 = 0.993$), 0.260 ($R^2 = 0.953$) and 0.240 ($R^2 = 0.976$) respectively (Fig. 10).

3.7. TD-DFT studies

3.7.1. Optimization of molecular structure

Computational studies were carried by using Density Functional Theory (DFT) to understand geometries of rhodol derivatives **10**, **11** and **12** with the method B3LYP/6-31 G (d). There is a variation in dihedral angles of the dyes in the geometries at the ground state as shown (Fig. 11).

All these dyes show significant variation in the dihedral angles at C3 and C6 position in xanthene part and N, N-diethyl amine part (137.73° to 176.68°). The compound **10** shows dihedral angle C6—C3—C17—C19 137.73° in spirocyclic form whereas in open form the dihedral angle in C6—C3—C17—C19 is 173.18°. Bond lengths are N27—C6 1.38 Å, C17—C19 1.52 Å, O45—C11 1.34 Å and C10—C49 1.46 Å in spirocyclic form of **10** whereas they are N25—C6 1.37 Å, C17—C18 1.50 Å, O43—C11 1.26 Å and C10—C46 1.46 Å in the open form of **10**. The compound **12** shows dihedral angle C6—C3—C17—C19 138.16° in spirocyclic form whereas in open form dihedral angle in C6—C3—C17—C19 is 176.68°. The bond lengths are N27—C6 1.38 Å, C17—C19 1.52 Å, O45—C11 1.34 Å and C10—C49 1.46 Å in spirocyclic

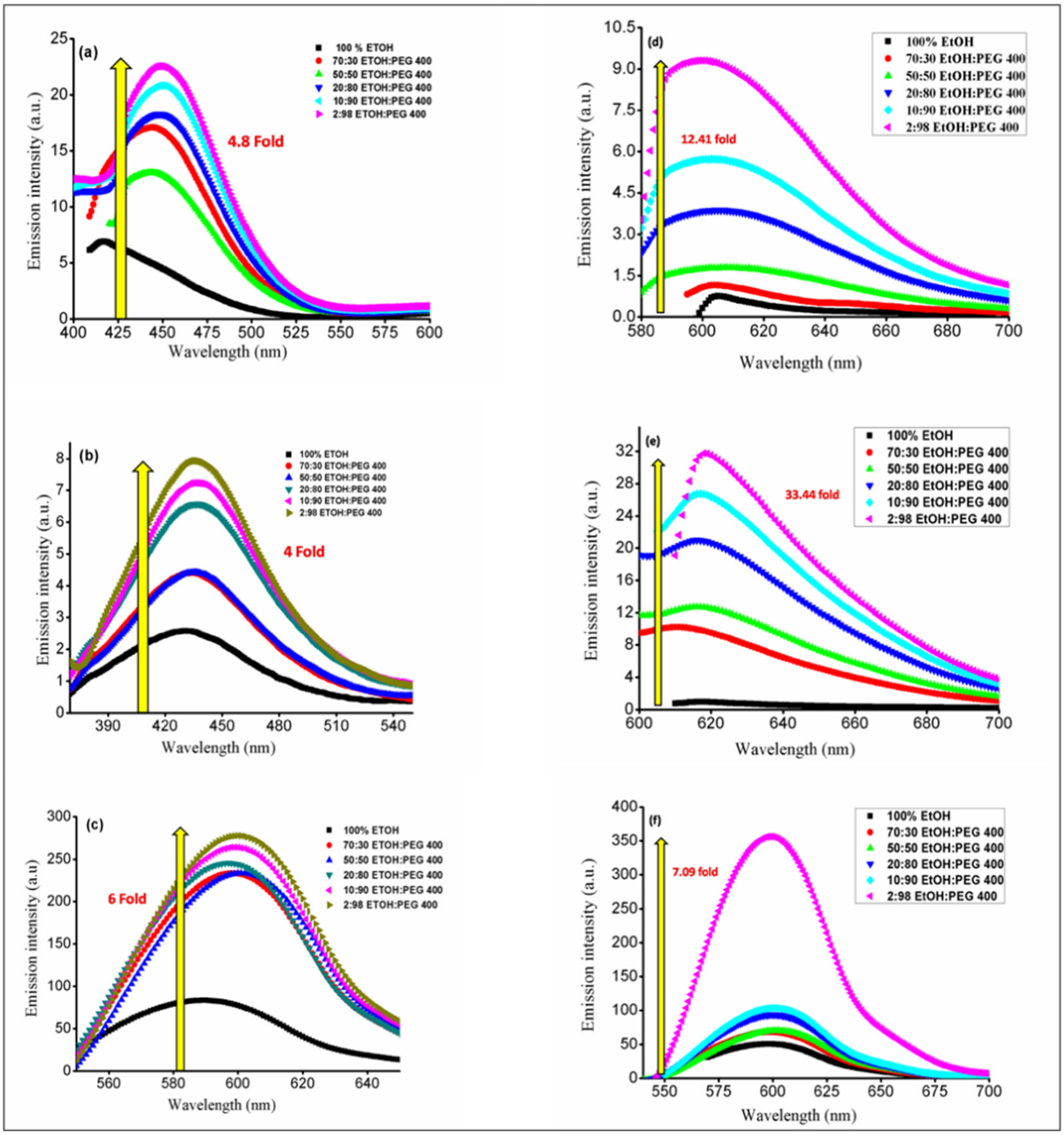

Fig. 9. Emission enhancement spectra of spirocyclic form - (a) **10**, (b) **11** and (c) **12** and open form - (d) **10**, (e) **11** and (f) **12** in different ratio of PEG 400 (0 to 100%) in ethanol at room temperature.

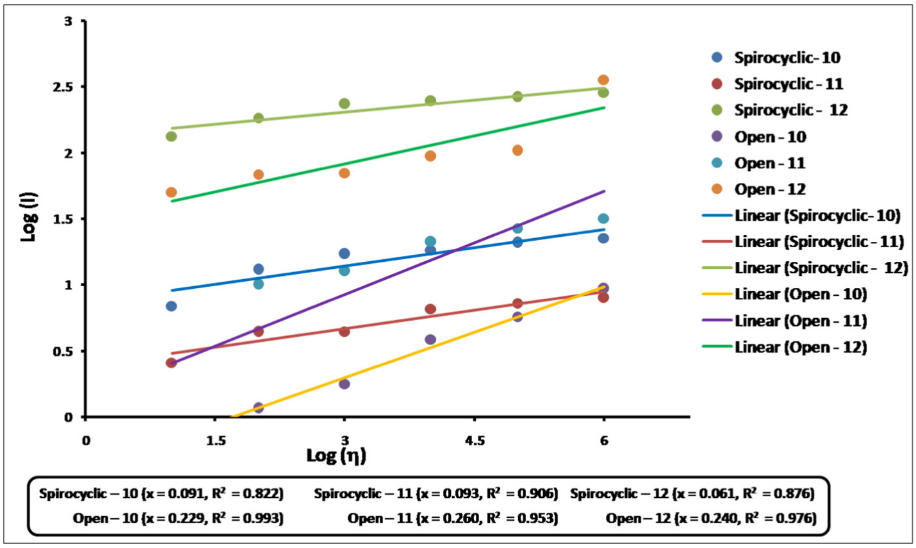

Fig. 10. Comparative Forster-Hoffman plot for compound **10**, **11** and **12**.

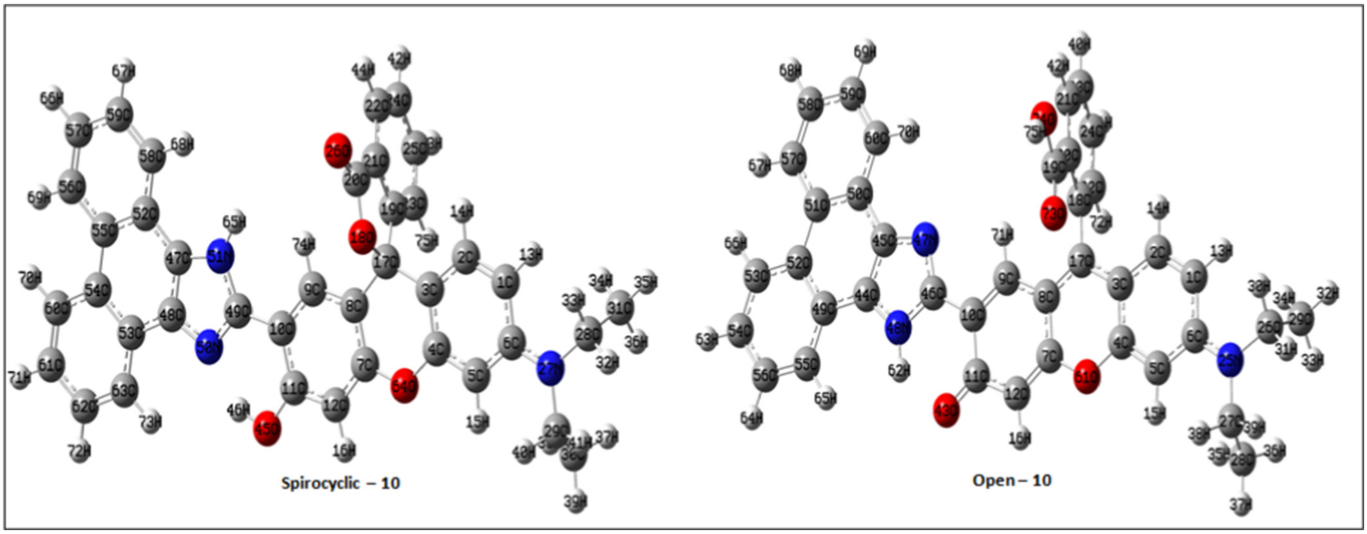

Fig. 11. Optimized structure of **10** in their spirocyclic and open form at B3LYP-6-31G (d) level in chloroform.

Table 8
Experimental and computational photophysical properties of **12** in their spirocyclic and open form.

Solvents	Experimental/computational (spirocyclic form)				Experimental/computational (open form)			
	λ_{abs}[a] (nm)	Vertical excitation[b]	f[c]	Major[d] orbital contribution	λ_{abs}[e] (nm)	λ_{abs}[f] (nm)	f[g]	Major[h] orbital contribution
Hexane	339	345.38	1.11	H → L (95.22%)	537	535.18	0.41	H → L (98%)
Toluene	340	346.44	2.14	H → L (95.22%)	539	539.96	0.72	H → L (98%)
$CHCl_3$	342	345.17	0.91	H → L (95.22%)	544	540.18	3.32	H → L (98%)
EA	341	344.11	2.65	H → L (95.22%)	545	545.99	0.16	H → L (98%)
MEOH	341	342.82	0.19	H → L (95.22%)	557	550.89	3.52	H → L (98%)
Dioxane	342	345.73	0.78	H → L (95.22%)	558	550.32	0.04	H → L (98%)
DMSO	343	343.84	0.75	H → L (95.22%)	574	559.48	0.86	H → L (98%)

[a] Experimental absorption λ_{max} of Spirocyclic form.
[b] Vertical excitation for spirocyclic form.
[c] Experimentally calculated oscillator strength for spirocyclic form.
[d] Major electronic transition from ground state to excited state for spirocyclic form.
[e] Experimental absorption λ_{max} of open form.
[f] Vertical excitation for open form.
[g] Experimentally calculated oscillator strength for open form.
[h] Major electronic transition from ground state to excited state for open form.

form of **12** whereas N26—C6 1.37 Å, C17—C19 1.50 Å, O44—C11 1.25 Å and C10—C45 1.46 Å in open form of **12**.

The observed changes in dihedral angle from spirocyclic form to open form lead to the co-planarity in the molecules. There are significant changes in bond length O45-C11 compared to the N- substituent compound which clearly indicates that H atom from OH itself modulate quinoid form. Hence, ESIPT process is inhibited in open form due to lack of protons in close proximity of benzimidazole and benzothiazole units during quinoid form.

In order to understand the solvatochromism in rhodol derivatives the ground state optimized geometries of the dyes at B3LYP/6-31 G (d) level were subjected to TD for the first 10 states in the solvents of different polarities to get the vertical excitations and results are tabulated in Table 8. The results obtained by TD-DFT suggested that there is a pronounced effect of solvent polarities on solvatochromism in rhodols.

Electron density in HOMOs is located on the xanthene part, benzimidazole, benzothiazole substituents and nitrogen atom, whereas in LUMOs were located on lactone part and extended over the benzimidazole and benzothiazole substituents in rhodol derivatives **10**, **11** and **12** in their both the forms. Fig. 12 shows the frontier molecular orbital (FMO) diagram of **10**, **11** and **12** in their spirocyclic and open forms in chloroform. Comparatively lower HOMO-LUMO energy gap is observed for the open form **10**, **11** and **12** than their respective spirocyclic forms which suggests a better ICT and red shifted emission in the open forms **10**, **11** and **12**.

We also studied separation of HOMO and LUMO energy levels in **10**, **11** and **12** in their spirocyclic and open forms. Fig. 13 shows the HOMO-LUMO energy gap diagram for **10**, **11** and **12**.

3.7.2. Molecular electrostatic potential plot (MEP)

The optimization of rhodol derivatives **10**, **11** and **12** in their spirocyclic and open form at B3LYP/6-31 G (d) level. We observed the exact reactive sites in molecules by molecular electrostatic potential (MEP) analysis [106]. In MEP surface plot the red colored area indicates

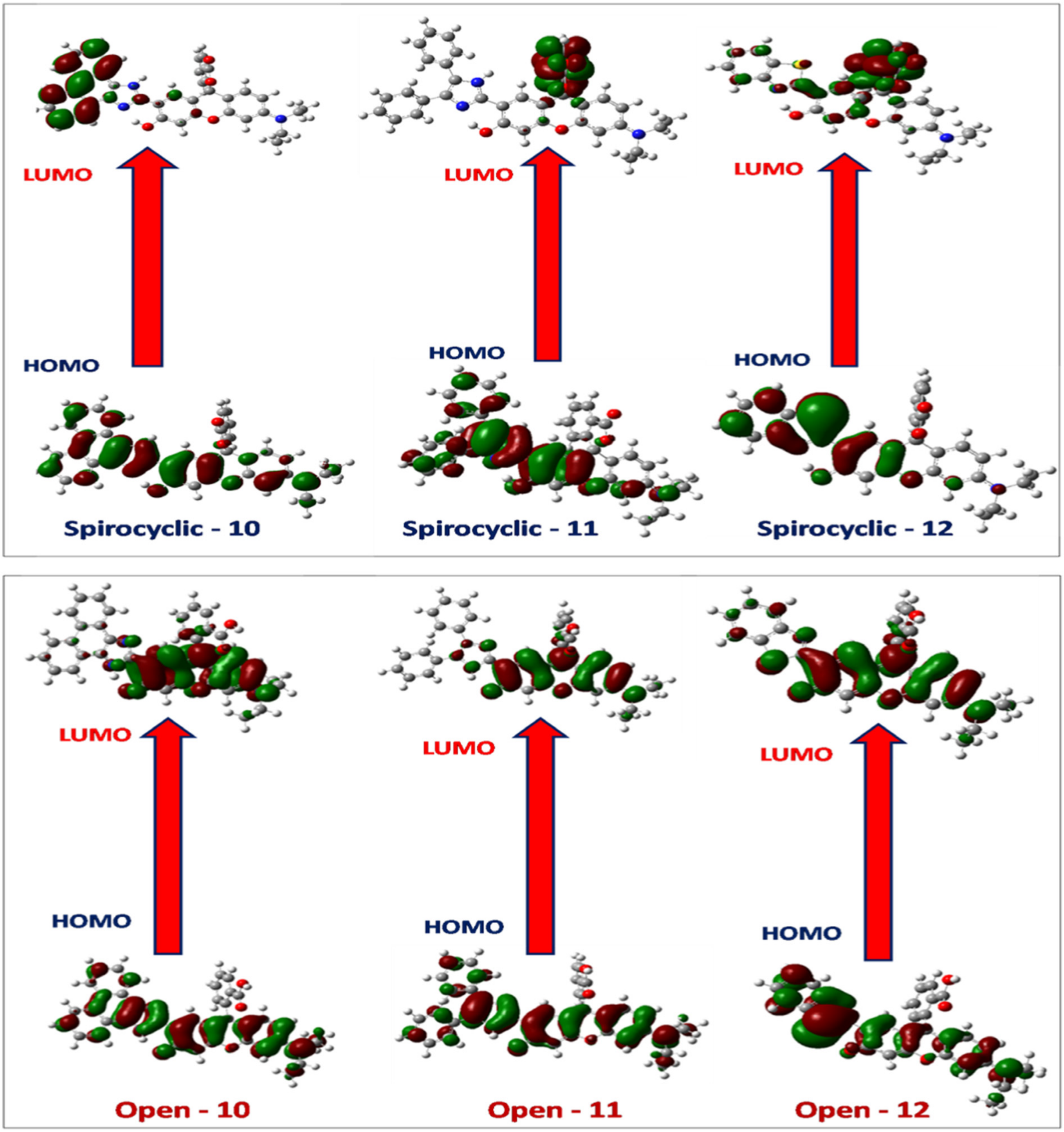

Fig. 12. HOMO-LUMO FMO diagrams for **10**, **11** and **12** (spirocyclic and open form) in chloroform.

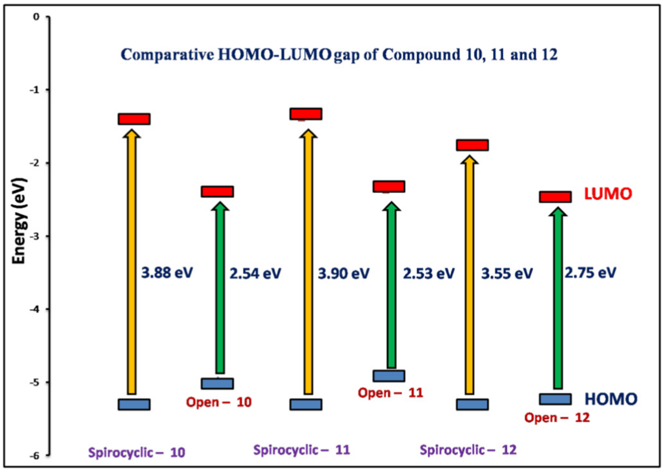

Fig. 13. HOMO-LUMO energy level diagram of **10**, **11** and **12** (spirocyclic and open form) in chloroform.

electron acceptor part whereas, the blue colored area indicates electron donor part in molecule. Fig. 14 shows the electrostatic potential characteristics through plots for **10**, **11** and **12** in their spirocyclic and open forms.

In spirocyclic form of **10** and **11** lactone group, and benzimidazole substituent act as electron acceptors, where as in **12** lactone group, and benzothiazole substituent act as electron acceptors. Therefore, in all spirocyclic form of **10**, **11** and **12** acceptor part have negative electron potential. The N, N-diethyl amine substituent in spirocyclic form of **10**, **11** and **12** acts as electron donors and has a positive electron potential.

Similarly, in the open form of **10** and **11** the quinoidal part and adjacent benzimidazole substituent acts as electron acceptors, whereas in **12** the quinoidal part and adjacent benzothiazole substituent act as an electron acceptors. Therefore, in all the open forms of **10**, **11** and **12** acceptor part have negative electron potential. The carboxyl (—COOH) group and N, N-diethyl amine substituent in open forms of **10**, **11** and **12** act as electron donor and have a positive electron potential. MEP observed for **10**, **11** and **12** in spirocyclic form are ±0.136, ±0.123, ±0.0999 and in open form are ±0.112, ±0.117, ±0.123 respectively.

4. Conclusion

Three rhodol compounds, namely spirolactamized phenanthrene-imidazole, diphenyl-imidazole and benzothiazole substituted N, N-diethylamine rhodols were synthesized to investigate their ESIPT phenomena. Detailed photophysical investigations of these dyes in their spirocyclic and open form are presented in a correlative manner. Due to ESIPT process, a large Stokes shift (50–260 nm) is observed in their spirocyclic form while no ESIPT process [Stokes shift 10–40 nm] is observed in their open form due to the lack of protons. Both Spirocyclic and open form shows positive solvatochromism which is supported by the linear analysis (Lippert-Mataga and Mac-Rae functions) as well as by using multi-linear regression analysis (Kamlet-Taft and Catalan parameters). The intramolecular charge transfer (ICT) and twisted intramolecular charge transfer (TICT) of synthesized rhodols were investigated using polarity graphs and Generalized Mulliken-Hush parameters (GMH) calculations. Moreover, open form of synthesized rhodols shows a high sensitivity towards viscous medium (mixture of EtOH:PEG 400) as compared to their spirocyclic form. The computational results obtained from DFT are in good agreement with the experimental results.

Acknowledgment

The authors Sagar B. Yadav and Shantaram Kothavale are grateful to UGC-SAP, New Delhi, India for financial support by way of Junior Research and Senior Research Fellowships. We are thankful to Mrs. Pallavi Khapre and Mrs. Priyanka Jain, Department of SAIF, IIT Bombay for mass analysis.

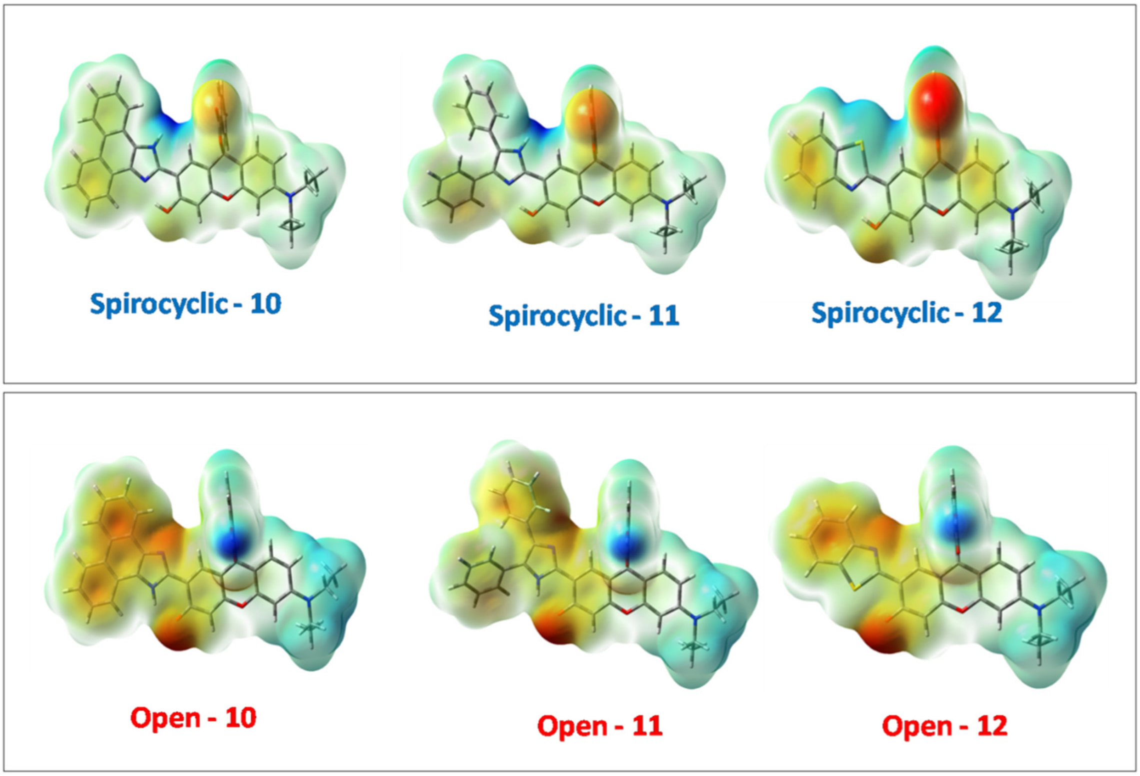

Fig. 14. MEP surface plot for **10**, **11** and **12** (spirocyclic and open form).

Appendix A. Supplementary data

Supplementary data to this article can be found online at https://doi.org/10.1016/j.molliq.2019.111626.

References

[1] H.M. Kim, B.R. Cho, Two-photon fluorescent probes for metal ions, Chem. - An Asian J. 6 (2011) 58–69, https://doi.org/10.1002/asia.201000542.

[2] H.M. Kim, H.-J. Choo, S.-Y. Jung, Y.-G. Ko, W.-H. Park, S.-J. Jeon, C.H. Kim, T. Joo, B.R. Cho, A two-photon fluorescent probe for lipid raft imaging: C-laurdan, ChemBioChem 8 (2007) 553–559, https://doi.org/10.1002/cbic.200700003.

[3] S. Sumalekshmy, C.J. Fahrni, Metal-ion-responsive fluorescent probes for two-photon excitation microscopy, Chem. Mater. 23 (2011) 483–500, https://doi.org/10.1021/cm1021905.

[4] Z. Liu, W. He, Z. Guo, Metal coordination in photoluminescent sensing, Chem. Soc. Rev. 42 (2013) 1568, https://doi.org/10.1039/c2cs35363f.

[5] L.E. Kreno, K. Leong, O.K. Farha, M. Allendorf, R.P. Van Duyne, J.T. Hupp, Metal–organic framework materials as chemical sensors, Chem. Rev. 112 (2012) 1105–1125, https://doi.org/10.1021/cr200324t.

[6] Y. Jeong, J. Yoon, Recent progress on fluorescent chemosensors for metal ions, Inorganica Chim. Acta. 381 (2012) 2–14, https://doi.org/10.1016/j.ica.2011.09.011.

[7] Y. Cui, Y. Yue, G. Qian, B. Chen, Luminescent functional metal–organic frameworks, Chem. Rev. 112 (2012) 1126–1162, https://doi.org/10.1021/cr200101d.

[8] X. Chen, T. Pradhan, F. Wang, J.S. Kim, J. Yoon, Fluorescent chemosensors based on spiroring-opening of xanthenes and related derivatives, Chem. Rev. 112 (2012) 1910–1956, https://doi.org/10.1021/cr200201z.

[9] Y. Yang, Q. Zhao, W. Feng, F. Li, Luminescent chemodosimeters for bioimaging, Chem. Rev. 113 (2013) 192–270, https://doi.org/10.1021/cr2004103.

[10] J.Y. Kwon, Y.J. Jang, Y.J. Lee, K.M. Kim, M.S. Seo, W. Nam, J. Yoon, A highly selective fluorescent chemosensor for Pb2+, J. Am. Chem. Soc. 127 (2005) 10107–10111, https://doi.org/10.1021/ja051075b.

[11] Y.-K. Yang, K.-J. Yook, J. Tae, A rhodamine-based fluorescent and colorimetric chemodosimeter for the rapid detection of Hg2+ ions in aqueous media, J. Am. Chem. Soc. 127 (2005) 16760–16761, https://doi.org/10.1021/ja054855t.

[12] M.H. Lee, J.-S. Wu, J.W. Lee, J.H. Jung, J.S. Kim, Highly sensitive and selective chemosensor for Hg2+ based on the rhodamine fluorophore, Org. Lett. 9 (2007) 2501–2504, https://doi.org/10.1021/ol0708931.

[13] S.-K. Ko, Y.-K. Yang, J. Tae, I. Shin, In vivo monitoring of mercury ions using a rhodamine-based molecular probe, J. Am. Chem. Soc. 128 (2006) 14150–14155, https://doi.org/10.1021/ja065114a.

[14] H. Zheng, Z.-H. Qian, L. Xu, F.-F. Yuan, L.-D. Lan, J.-G. Xu, Switching the recognition preference of rhodamine B spirolactam by replacing one atom: design of rhodamine B thiohydrazide for recognition of Hg(II) in aqueous solution, Org. Lett. 8 (2006) 859–861, https://doi.org/10.1021/ol0529086.

[15] Y. Xiang, A. Tong, P. Jin, Y. Ju, New fluorescent rhodamine hydrazone chemosensor for Cu(II) with high selectivity and sensitivity, Org. Lett. 8 (2006) 2863–2866, https://doi.org/10.1021/ol0610340.

[16] X. Zhang, Y. Shiraishi, T. Hirai, Cu(II)-selective green fluorescence of a rhodamine–diacetic acid conjugate, Org. Lett. 9 (2007) 5039–5042, https://doi.org/10.1021/ol7022714.

[17] Y. Xiang, A. Tong, A new rhodamine-based chemosensor exhibiting selective FeIII-amplified fluorescence, Org. Lett. 8 (2006) 1549–1552, https://doi.org/10.1021/ol060001h.

[18] S. Bae, J. Tae, Rhodamine-hydroxamate-based fluorescent chemosensor for FeIII, Tetrahedron Lett. 48 (2007) 5389–5392, https://doi.org/10.1016/j.tetlet.2007.06.014.

[19] X. Zhang, Y. Shiraishi, T. Hirai, A new rhodamine-based fluorescent chemosensor for transition metal cations synthesized by one-step facile condensation, Tetrahedron Lett. 48 (2007) 5455–5459, https://doi.org/10.1016/j.tetlet.2007.05.171.

[20] M. Beija, C.A.M. Afonso, J.M.G. Martinho, Synthesis and applications of Rhodamine derivatives as fluorescent probes, Chem. Soc. Rev. 38 (2009) 2410–2433, https://doi.org/10.1039/b901612k.

[21] Y. Koide, Y. Urano, K. Hanaoka, T. Terai, T. Nagano, Evolution of group 14 rhodamines as platforms for near-infrared fluorescence probes utilizing photoinduced electron transfer, ACS Chem. Biol. 6 (2011) 600–608, https://doi.org/10.1021/cb1002416.

[22] J.B. Grimm, A.J. Sung, W.R. Legant, P. Hulamm, S.M. Matlosz, E. Betzig, L.D. Lavis, Carbo fl uoresceins and carborhodamines as scaffolds for high-contrast fluorogenic probes, (2013).

[23] X. Zhang, Y. Xiao, X. Qian, A ratiometric fluorescent probe based on FRET for imaging Hg2+ ions in living cells, Angew. Chemie - Int. Ed. 47 (2008) 8025–8029, https://doi.org/10.1002/anie.200803246.

[24] A. Thorne, An introduction to laser spectroscopy, Meas. Sci. Technol. 7 (1996) http://stacks.iop.org/0957-0233/7/i=11/a=022.

[25] P. Yang, J. Zhao, W. Wu, X. Yu, Y. Liu, Accessing the long-lived triplet excited states in bodipy-conjugated 2-(2-hydroxyphenyl) benzothiazole/benzoxazoles and applications as organic triplet photosensitizers for photooxidations, J. Org. Chem. 77 (2012) 6166–6178, https://doi.org/10.1021/jo300943t.

[26] Y. Houari, S. Chibani, D. Jacquemin, A.D. Laurent, TD-DFT assessment of the excited state intramolecular proton transfer in hydroxyphenylbenzimidazole (HBI) dyes, J. Phys. Chem. B 119 (2015) 2180–2192, https://doi.org/10.1021/jp505036d.

[27] L. Xie, Y. Chen, W. Wu, H. Guo, J. Zhao, X. Yu, Fluorescent coumarin derivatives with large stokes shift, dual emission and solid state luminescent properties: an experimental and theoretical study, Dyes Pigments 92 (2012) 1361–1369, https://doi.org/10.1016/j.dyepig.2011.09.023.

[28] S. Barman, S.K. Mukhopadhyay, M. Gangopadhyay, S. Biswas, S. Dey, N.D.P. Singh, Coumarin-benzothiazole-chlorambucil (Cou-Benz-Cbl) conjugate: an ESIPT based pH sensitive photoresponsive drug delivery system, J. Mater. Chem. B 3 (2015) 3490–3497, https://doi.org/10.1039/c4tb02081b.

[29] A.Y. Bochkov, I.O. Akchurin, O.A. Dyachenko, V.F. Traven, NIR-fluorescent coumarin-fused BODIPY dyes with large Stokes shifts, Chem. Commun. 49 (2013) 11653–11655, https://doi.org/10.1039/c3cc46498a.

[30] I. Esnal, G. Duran-Sampedro, A.R. Agarrabeitia, J. Bañuelos, I. García-Moreno, M.A. Macías, E. Peña-Cabrera, I. López-Arbeloa, S. De La Moya, M.J. Ortiz, Coumarin-BODIPY hybrids by heteroatom linkage: versatile, tunable and photostable dye lasers for UV irradiation, Phys. Chem. Chem. Phys. 17 (2015) 8239–8247, https://doi.org/10.1039/c5cp00193e.

[31] H. Yu, L. Jin, Y. Dai, H. Li, Y. Xiao, From a BODIPY–rhodamine scaffold to a ratiometric fluorescent probe for nitric oxide, New J. Chem. 37 (2013) 1688–1691, https://doi.org/10.1039/C3NJ41127C.

[32] C. Ram, S. Sivamani, T. Micha Premkumar, V. Hariram, Computational study of leading edge jet impingement cooling with a conical converging hole for blade cooling, ARPN J. Eng. Appl. Sci. 12 (2017) 6397–6406, https://doi.org/10.1039/b000000x.

[33] J. Chen, W. Liu, B. Zhou, G. Niu, H. Zhang, J. Wu, Y. Wang, W. Ju, P. Wang, Coumarin- and rhodamine-fused deep red fluorescent dyes: synthesis, photophysical properties, and bioimaging in vitro, J. Org. Chem. 78 (2013) 6121–6130, https://doi.org/10.1021/jo400783x.

[34] S. Kothavale, N. Sekar, Novel triphenylamine based rhodamine derivatives: synthesis, characterization, photophysical properties and viscosity sensitivity, RSC Adv. 6 (2016) 100271–100280, https://doi.org/10.1039/c6ra19899f.

[35] B.K. Paul, N. Guchhait, 1-Hydroxy-2-naphthaldehyde: a prospective excited-state intramolecular proton transfer (ESIPT) probe with multi-faceted applications, J. Lumin. 132 (2012) 2194–2208, https://doi.org/10.1016/j.jlumin.2012.03.036.

[36] L. Fan, X. Jiang, B. Wang, Z. Yang, 4-(8′-Hydroxyquinolin-7′-yl)methyleneimino-1-phenyl-2,3-dimethyl-5-pyzole as a fluorescent chemosensor for aluminum ion in acid aqueous medium, Sensors Actuators B Chem. 205 (2014) 249–254, https://doi.org/10.1016/j.snb.2014.08.085.

[37] L. Tang, Z. Zheng, K. Zhong, Y. Bian, A 2,5-diaryl-1,3,4-oxadiazole-based fluorescent probe for rapid and highly selective recognition of hydrogen sulfide with a large Stokes shift through switching on ESIPT, Tetrahedron Lett. 57 (2016) 1361–1364, https://doi.org/10.1016/j.tetlet.2016.02.056.

[38] B. Gu, L. Huang, W. Su, X. Duan, H. Li, S. Yao, A benzothiazole-based fluorescent probe for distinguishing and bioimaging of Hg2+ and Cu2+, Anal. Chim. Acta 954 (2017) 97–104, https://doi.org/10.1016/j.aca.2016.11.044.

[39] D. Xu, L. Tang, M. Tian, P. He, X. Yan, A benzothizole-based fluorescent probe for Hg2+ recognition utilizing ESIPT coupled AIE characteristics, Tetrahedron Lett. 58 (2017) 3654–3657, https://doi.org/10.1016/j.tetlet.2017.08.016.

[40] S. Chen, W. Wang, M. Yan, Q. Tu, S.-W. Chen, T. Li, M.-S. Yuan, J. Wang, 2-Hydroxy benzothiazole modified rhodol: aggregation-induced emission and dual-channel fluorescence sensing of Hg2+ and Ag+ ions, Sensors Actuators B Chem. 255 (2018) 2086–2094, https://doi.org/10.1016/j.snb.2017.09.008.

[41] J. Wu, W. Liu, J. Ge, H. Zhang, P. Wang, New sensing mechanisms for design of fluorescent chemosensors emerging in recent years, Chem. Soc. Rev. 40 (2011) 3483, https://doi.org/10.1039/c0cs00224k.

[42] T. Mutai, H. Sawatani, T. Shida, H. Shono, K. Araki, Tuning of excited-state intramolecular proton transfer (ESIPT) fluorescence of Imidazo[1,2-a]pyridine in rigid matrices by substitution effect, J. Org. Chem. 78 (2013) 2482–2489, https://doi.org/10.1021/jo302711t.

[43] Y. Liu, D. Yu, S. Ding, Q. Xiao, J. Guo, G. Feng, Rapid and ratiometric fluorescent detection of cysteine with high selectivity and sensitivity by a simple and readily available probe, ACS Appl. Mater. Interfaces 6 (2014) 17543–17550, https://doi.org/10.1021/am505501d.

[44] K. Kanagaraj, K. Pitchumani, Highly selective “turn-on” fluorescent and colorimetric sensing of fluoride ion using 2-(2-hydroxyphenyl)-2,3-dihydroquinolin-4(1H)-one based on excited-state proton transfer, Chem. - An Asian J. 9 (2014) 146–152, https://doi.org/10.1002/asia.201300816.

[45] Y. Zhang, J.-H. Wang, W. Zheng, T. Chen, Q.-X. Tong, D. Li, An ESIPT fluorescent dye based on HBI with high quantum yield and large Stokes shift for selective detection of Cys, J. Mater. Chem. B 2 (2014) 4159–4166, https://doi.org/10.1039/C4TB00190G.

[46] B. Liu, H. Wang, T. Wang, Y. Bao, F. Du, J. Tian, Q. Li, R. Bai, A new ratiometric ESIPT sensor for detection of palladium species in aqueous solution, Chem. Commun. 48 (2012) 2867, https://doi.org/10.1039/c2cc17677g.

[47] W.-H. Chen, Y. Xing, Y. Pang, A highly selective pyrophosphate sensor based on ESIPT turn-on in water, Org. Lett. 13 (2011) 1362–1365, https://doi.org/10.1021/ol200054w.

[48] X.-F. Yang, H. Qi, L. Wang, Z. Su, G. Wang, A ratiometric fluorescent probe for fluoride ion employing the excited-state intramolecular proton transfer, Talanta 80 (2009) 92–97, https://doi.org/10.1016/j.talanta.2009.06.030.

[49] F. Rodriguez Prieto, M.C. Rios Rodriguez, M. Mosquera Gonzalez, M.A. Rios Fernandez, Ground- and excited-state tautomerism in 2-(3′-hydroxy-2′-pyridyl) benzimidazole, J. Phys. Chem. 98 (1994) 8666–8672, https://doi.org/10.1021/j100086a014.

[50] M. Mosquera, M.C. Ríos Rodríguez, F. Rodríguez-Prieto, Competition between protonation and deprotonation in the first excited singlet state of 2-(3′-hydroxy-2′-pyridyl)benzimidazole in acidic solutions, J. Phys. Chem. A 101 (1997) 2766–2772, https://doi.org/10.1021/jp9626834.

[51] S. Li, Q. Wang, Y. Qian, S. Wang, Y. Li, G. Yang, Understanding the pressure-induced emission enhancement for triple fluorescent compound with excited-state

intramolecular proton transfer, J. Phys. Chem. A 111 (2007) 11793–11800, https://doi.org/10.1021/jp075301a.

[52] R. Hu, J. Feng, D. Hu, S. Wang, S. Li, Y. Li, G. Yang, A rapid aqueous fluoride ion sensor with dual output modes, Angew. Chemie Int. Ed. 49 (2010) 4915–4918, https://doi.org/10.1002/anie.201000790.

[53] T.-I. Kim, H.J. Kang, G. Han, S.J. Chung, Y. Kim, A highly selective fluorescent ESIPT probe for the dual specificity phosphatase MKP-6, Chem. Commun. (2009) 5895, https://doi.org/10.1039/b911145j.

[54] S. Goswami, S. Das, K. Aich, B. Pakhira, S. Panja, S.K. Mukherjee, S. Sarkar, A chemodosimeter for the ratiometric detection of hydrazine based on return of ESIPT and its application in live-cell imaging, Org. Lett. 15 (2013) 5412–5415, https://doi.org/10.1021/ol4026759.

[55] Z. Xu, L. Xu, J. Zhou, Y. Xu, W. Zhu, X. Qian, A highly selective fluorescent probe for fast detection of hydrogen sulfide in aqueous solution and living cells, Chem. Commun. 48 (2012), 10871. https://doi.org/10.1039/c2cc36141h.

[56] L. Cui, W. Zhu, Y. Xu, X. Qian, A novel ratiometric sensor for the fast detection of palladium species with large red-shift and high resolution both in aqueous solution and solid state, Anal. Chim. Acta 786 (2013) 139–145, https://doi.org/10.1016/j.aca.2013.05.011.

[57] M. Santra, B. Roy, K.H. Ahn, A “reactive” ratiometric fluorescent probe for mercury species, Org. Lett. 13 (2011) 3422–3425, https://doi.org/10.1021/ol2011693.

[58] C. Huang, T. Jia, C. Yu, A. Zhang, N. Jia, An ESIPT based fluorescent probe for highly selective and ratiometric detection of periodate, Biosens. Bioelectron. 63 (2015) 513–518, https://doi.org/10.1016/j.bios.2014.08.005.

[59] D.P. Murale, H. Kim, W.S. Choi, D.G. Churchill, Highly selective excited state intramolecular proton transfer (ESIPT)-based superoxide probing, Org. Lett. 15 (2013) 3946–3949, https://doi.org/10.1021/ol4017222.

[60] G. Li, D. Zhu, Q. Liu, L. Xue, H. Jiang, Rapid detection of hydrogen peroxide based on aggregation induced ratiometric fluorescence change, Org. Lett. 15 (2013) 924–927, https://doi.org/10.1021/ol4000845.

[61] D. Maity, V. Kumar, T. Govindaraju, Reactive probes for ratiometric detection of Co2 + and Cu+ based on excited-state intramolecular proton transfer mechanism, Org. Lett. 14 (2012) 6008–6011, https://doi.org/10.1021/ol302904c.

[62] L. Xiong, J. Feng, R. Hu, S. Wang, S. Li, Y. Li, G. Yang, Sensing in 15 s for aqueous fluoride anion by water-insoluble fluorescent probe incorporating hydrogel, Anal. Chem. 85 (2013) 4113–4119, https://doi.org/10.1021/ac400252u.

[63] S. Jana, S. Dalapati, N. Guchhait, Proton transfer assisted charge transfer phenomena in photochromic Schiff bases and effect of –NEt 2 groups to the anil Schiff bases, J. Phys. Chem. A 116 (2012) 10948–10958, https://doi.org/10.1021/jp3079698.

[64] J.E. Kwon, S.Y. Park, Advanced organic optoelectronic materials: harnessing excited-state intramolecular proton transfer (ESIPT) process, Adv. Mater. 23 (2011) 3615–3642, https://doi.org/10.1002/adma.201102046.

[65] L. Giordano, V. V Shvadchak, J.A. Fauerbach, E.A. Jares-Erijman, T.M. Jovin, Highly solvatochromic 7-aryl-3-hydroxychromones, J. Phys. Chem. Lett. 3 (2012) 1011–1016. doi:https://doi.org/10.1021/jz3002019.

[66] S. Kim, S.Y. Park, Photochemically gated protonation effected by intramolecular hydrogen bonding: towards stable fluorescence imaging in polymer films, Adv. Mater. 15 (2003) 1341–1344, https://doi.org/10.1002/adma.200305050.

[67] S. Kim, S.Y. Park, I. Yoshida, H. Kawai, T. Nagamura, Amplified spontaneous emission from the film of poly(aryl ether) dendrimer encapsulating excited-state intramolecular proton transfer dye, J. Phys. Chem. B 106 (2002) 9291–9294, https://doi.org/10.1021/jp021048x.

[68] P. Osa, vol. 3. Osnovni principi solarne geometrije, (n.d).

[69] S. Kenmoku, Y. Urano, H. Kojima, T. Nagano, Development of a highly specific rhodamine-based fluorescence probe for hypochlorous acid and its application to real-time imaging of phagocytosis, J. Am. Chem. Soc. 129 (2007) 7313–7318, https://doi.org/10.1021/ja068740g.

[70] J. Wu, Z. Ye, F. Wu, H. Wang, L. Zeng, G.-M. Bao, A rhodamine-based fluorescent probe for colorimetric and fluorescence lighting-up determination of toxic thiophenols in environmental water and living cells, Talanta 181 (2018) 239–247, https://doi.org/10.1016/j.talanta.2018.01.028.

[71] K. Wechakorn, S. Prabpai, K. Suksen, P. Piyachaturawat, P. Kongsaeree, Rhodol-based fluorescent probe for Au3+ detection and its application in bioimaging, RSC Adv. 6 (2016) 24752–24755, https://doi.org/10.1039/C6RA02342H.

[72] X.-F. Yang, Q. Huang, Y. Zhong, Z. Li, H. Li, M. Lowry, J.O. Escobedo, R.M. Strongin, A dual emission fluorescent probe enables simultaneous detection of glutathione and cysteine/homocysteine, Chem. Sci. 5 (2014) 2177, https://doi.org/10.1039/c4sc00308j.

[73] H. Wen, Q. Huang, X.-F. Yang, H. Li, Spirolactamized benzothiazole-substituted N, N-diethylrhodol: a new platform to construct ratiometric fluorescent probes, Chem. Commun. 49 (2013) 4956, https://doi.org/10.1039/c3cc41343h.

[74] D. Raghavender Goud, A.K. Purohit, V. Tak, D.K. Dubey, P. Kumar, D. Pardasani, A highly selective and sensitive “turn-on” fluorescence chemodosimeter for the detection of mustard gas, Chem. Commun. 50 (2014) 12363–12366, https://doi.org/10.1039/C4CC04801F.

[75] H. Wen, Q. Huang, X.-F. Yang, H. Li, Spirolactamized benzothiazole-substituted N, N-diethylrhodol: a new platform to construct ratiometric fluorescent probes, Chem. Commun. 49 (2013) 4956, https://doi.org/10.1039/c3cc41343h.

[76] A. Manna, D. Sarkar, S. Goswami, C.K. Quah, H.-K. Fun, Single excited state intramolecular proton transfer (ESIPT) chemodosimeter based on rhodol for both Hg2+ and OCl−: ratiometric detection with live-cell imaging, RSC Adv. 6 (2016) 57417–57423, https://doi.org/10.1039/C6RA11009F.

[77] Y. Liu, K. Xiang, B. Tian, J. Zhang, Rhodol-based far-red fluorescent probe for the detection of cysteine and homocysteine over glutathione, Luminescence 32 (2017) 78–85, https://doi.org/10.1002/bio.3152.

[78] X.-F. Yang, Q. Huang, Y. Zhong, Z. Li, H. Li, M. Lowry, J.O. Escobedo, R.M. Strongin, A dual emission fluorescent probe enables simultaneous detection of glutathione and cysteine/homocysteine, Chem. Sci. 5 (2014) 2177, https://doi.org/10.1039/c4sc00308j.

[79] W. Kohn, L.J. Sham, Self-consistent equations including exchange and correlation effects, Phys. Rev. 140 (1965) A1133–A1138, https://doi.org/10.1103/PhysRev.140.A1133.

[80] J.H.M.J. Frisch, G.W. Trucks, H.B. Schlegel, G.E. Scuseria, M.A. Robb, J.R. Cheeseman, G. Scalmani, V. Barone, B. Mennucci, G.A. Petersson, H. Nakatsuji, M. Caricato, X. Li, H.P. Hratchian, A.F. Izmaylov, J. Bloino, G. Zheng, J.L. Sonnenberg, M. Had, Gaussian 09, Gaussian, Inc., Wallingford CT, 2009.

[81] A.D. Becke, A new mixing of Hartree–Fock and local density-functional theories, J. Chem. Phys. 98 (1993) 1372–1377, https://doi.org/10.1063/1.464304.

[82] C. Lee, W. Yang, R.G. Parr, Development of the Colle-Salvetti correlation-energy formula into a functional of the electron density, Phys. Rev. B 37 (1988) 785–789, https://doi.org/10.1103/PhysRevB.37.785.

[83] G. Scalmani, M.J. Frisch, B. Mennucci, J. Tomasi, R. Cammi, V. Barone, Geometries and properties of excited states in the gas phase and in solution: theory and application of a time-dependent density functional theory polarizable continuum model, J. Chem. Phys. 124 (2006), 094107. https://doi.org/10.1063/1.2173258.

[84] A.G. Jadhav, S. Kothavale, N. Sekar, Red emitting triphenylamine based rhodamine analogous with enhanced Stokes shift and viscosity sensitive emission, Dyes Pigments 138 (2017) 56–67, https://doi.org/10.1016/j.dyepig.2016.11.021.

[85] W. Lin, Y. Liu, F. Meng, Q. Shi, Fluorescent Probe for Specific Identification of Divalent Copper Ions in Water Phase, 2015.

[86] H.R. Shaterian, M. Ranjbar, An environmental friendly approach for the synthesis of highly substituted imidazoles using Brønsted acidic ionic liquid, N-methyl-2-pyrrolidonium hydrogen sulfate, as reusable catalyst, J. Mol. Liq. 160 (2011) 40–49, https://doi.org/10.1016/j.molliq.2011.02.012.

[87] V.S. Patil, V.S. Padalkar, A.B. Tathe, V.D. Gupta, N. Sekar, Synthesis, photo-physical and DFT studies of ESIPT inspired novel 2-(2′,4′-dihydroxyphenyl) benzimidazole, benzoxazole and benzothiazole, J. Fluoresc. 23 (2013) 1019–1029, https://doi.org/10.1007/s10895-013-1228-4.

[88] S. Kothavale, N. Sekar, Novel pyrazino-phenanthroline based rigid donor-π-acceptor compounds: a detail study of optical properties, acidochromism, solvatochromism and structure-property relationship, Dyes Pigments 136 (2017) 31–45, https://doi.org/10.1016/j.dyepig.2016.08.032.

[89] S. Kothavale, A.G. Jadhav, N. Sekar, Deep red emitting triphenylamine based coumarin-rhodamine hybrids with large Stokes shift and viscosity sensing: synthesis, photophysical properties and DFT studies of their spirocyclic and open forms, Dyes Pigments 137 (2017) 329–341, https://doi.org/10.1016/j.dyepig.2016.11.010.

[90] C. Reichardt, Solvatochromic dyes as solvent polarity indicators, Chem. Rev. 94 (1994) 2319–2358, https://doi.org/10.1021/cr00032a005.

[91] S.K. Lanke, N. Sekar, Aggregation induced emissive carbazole-based push pull NLOphores: synthesis, photophysical properties and DFT studies, Dyes Pigments 124 (2016) 82–92, https://doi.org/10.1016/j.dyepig.2015.09.013.

[92] E.G. McRae, Theory of solvent effects on molecular electronic spectra. Frequency shifts, J. Phys. Chem. 61 (1957) 562–572, https://doi.org/10.1021/j150551a012.

[93] S.B. Yadav, S. Kothavale, N. Sekar, Triphenylamine and N-phenyl carbazole-based coumarin derivatives: synthesis, solvatochromism, acidochromism, linear and nonlinear optical properties, J. Photochem. Photobiol. A Chem. 382 (2019), 111937. https://doi.org/10.1016/j.jphotochem.2019.111937.

[94] B.J. Coe, J. Fielden, S.P. Foxon, J.A. Harris, M. Helliwell, B.S. Brunschwig, I. Asselberghs, K. Clays, J. Garín, J. Orduna, Diquat derivatives: highly active, two-dimensional nonlinear optical chromophores with potential redox switchability, J. Am. Chem. Soc. 132 (2010) 10498–10512, https://doi.org/10.1021/ja103289a.

[95] S.M. Abernathy, R.R. Sharp, Spin dynamics calculations of electron and nuclear spin relaxation times in paramagnetic solutions, J. Chem. Phys. 106 (1997) 9032–9043, https://doi.org/10.1063/1.474035.

[96] C. Creutz, M.D. Newton, N. Sutin, Metal—lingad and metal—metal coupling elements, J. Photochem. Photobiol. A Chem. 82 (1994) 47–59, https://doi.org/10.1016/1010-6030(94)02013-2.

[97] M.J. Kamlet, R.W. Taft, The solvatochromic comparison method. I. The .beta.-scale of solvent hydrogen-bond acceptor (HBA) basicities, J. Am. Chem. Soc. 98 (1976) 377–383, https://doi.org/10.1021/ja00418a009.

[98] M.J. Kamlet, J.L. Abboud, R.W. Taft, The solvatochromic comparison method. 6. The .pi.* scale of solvent polarities, J. Am. Chem. Soc. 99 (1977) 6027–6038, https://doi.org/10.1021/ja00460a031.

[99] J. Catalán, V. López, P. Pérez, R. Martin-Villamil, J.-G. Rodríguez, Progress towards a generalized solvent polarity scale: the solvatochromism of 2-(dimethylamino)-7-nitrofluorene and its homomorph 2-fluoro-7-nitrofluorene, Liebigs Ann. 1995 (1995) 241–252, https://doi.org/10.1002/jlac.199519950234.

[100] J. Catalán, C. Díaz, Extending the solvent acidity scale to highly acidic organic solvents: the unique photophysical behaviour of 3,6-diethyltetrazine, European J. Org. Chem. (1999) (1999) 885–891, https://doi.org/10.1002/(SICI)1099-0690(199904)1999:4<885::AID-EJOC885>3.0.CO;2-W.

[101] J. Catalán, H. Hopf, Empirical treatment of the inductive and dispersive components of solute—solvent interactions: the solvent polarizability (SP) scale, European J. Org. Chem. 2004 (2004) 4694–4702, https://doi.org/10.1002/ejoc.200400311.

[102] R.W. Taft, M.J. Kamlet, The solvatochromic comparison method. 2. The .alpha.-scale of solvent hydrogen-bond donor (HBD) acidities, J. Am. Chem. Soc. 98 (1976) 2886–2894, https://doi.org/10.1021/ja00426a036.

[103] J. Catalán, Toward a generalized treatment of the solvent effect based on four empirical scales: dipolarity (SdP, a new scale), polarizability (SP), acidity (SA), and basicity (SB) of the medium, J. Phys. Chem. B 113 (2009) 5951–5960, https://doi.org/10.1021/jp8095727.

[104] W. Rettig, Charge separation in excited states of decoupled systems?TICT compounds and implications regarding the development of new laser dyes and the primary process of vision and photosynthesis, Angew. Chemie Int. Ed. English. 25 (1986) 971–988, https://doi.org/10.1002/anie.198609711.

[105] M.A. Haidekker, E.A. Theodorakis, Molecular rotors—fluorescent biosensors for viscosity and flow, Org. Biomol. Chem. 5 (2007) 1669–1678, https://doi.org/10.1039/B618415D.

[106] M. Zouaoui-Rabah, M. Sekkal-Rahal, F. Djilani-Kobibi, A.M. Elhorri, M. Springborg, Performance of hybrid DFT compared to MP2 methods in calculating nonlinear optical properties of divinylpyrene derivative molecules, J. Phys. Chem. A 120 (2016) 8843–8852, https://doi.org/10.1021/acs.jpca.6b08040.